NASA

Advanced Ceramic Material for High Temperature Turbine Tip Seals

Final Report

By

J.W. Vogan, N.G. Solomon, and A.R.Stetson

SOLAR TURBINES INTERNATIONAL
An Operating Group of International Harvester

January 1980

Prepared for

NATIONAL AERONAUTICS AND SPACE ADMINISTRATION
NASA Lewis Research Center

Contract NAS3-20081

1. Report No.	2. Government Accession No.	3. Recipient's Catalog No.
CR-159774		

4. Title and Subtitle	5. Report Date
ADVANCED CERAMIC MATERIAL FOR HIGH TEMPERATURE TURBINE TIP SEALS	November 1979
	6. Performing Organization Code
7. Author(s)	8. Performing Organization Report No.
J. W. Vogan, N. G. Solomon, and A. R. Stetson	SR79-R-4482-43 (RDR 1831-43)
	10. Work Unit No.
9. Performing Organization Name and Address Solar Turbines International An Operating Group of International Harvester 2200 Pacific Highway, P.O. Box 80966 San Diego, California 92138	11. Contract or Grant No. NAS3-20081
	13. Type of Report and Period Covered Final, 2/76 - 5/79
12. Sponsoring Agency Name and Address National Aeronautics and Space Administration, Washington, DC 20546	14. Sponsoring Agency Code

15. Supplementary Notes

Project Manager, S. G. Young
NASA - Lewis Research Center (23-2)
Cleveland, Ohio 44135

16. Abstract

Forty-one material systems were evaluated for potential use in turbine blade tip seal applications at 1370 °C. Both ceramic blade tip inserts and abradable ceramic tip shoes were tested. Hot gas erosion, impact resistance, thermal stability and dynamic rub performance were the criteria used in rating the various materials. Abradability testing was conducted at selected blade tip speeds and interference rates over a temperature span of ambient to 1370 °C. Silicon carbide and silicon nitride were used, both as blade tips and abradables. The blade tip inserts were fabricated by hot pressing while low-density and honeycomb abradables were sintered or reaction bonded.

Results of the testing and analytical study demonstrated that silicon nitride blade tips could be incorporated into a production blade to provide improved wear resistance. It was also found that ceramic honeycomb abradable structures performed well in all tests, but specimen quality was subject to variation. Near the end of the program one vendor developed techniques for producing very uniform silicon carbide ceramic honeycomb components.

A technique was developed to braze reaction bonded silicon nitride honeycomb to hot-pressed silicon nitride. Effective braze alloys were pure silicon and silicon titanium alloys with up to 10 percent titanium.

The development and optimization of silicon nitride and silicon carbide abradable structures should be pursued. Improvements made in processing of ceramics since the inception of this program warrant further study.

17. Key Words (Suggested by Author(s))	18. Distribution Statement
Seals, Abradable, Turbine Blade, Ceramic, Silicon Nitride, Silicon Carbide	Unclassified - Unlimited

19. Security Classif. (of this report)	20. Security Classif. (of this page)	21. No. of Pages	22. Price*
Unclassified	Unclassified	85	

* For sale by the National Technical Information Service, Springfield, Virginia 22161

TABLE OF CONTENTS

TABLE OF CONTENTS (Cont)

LIST OF FIGURES

LIST OF FIGURES (Cont)

LIST OF FIGURES (Cont)

LIST OF FIGURES (Cont)

LIST OF FIGURES (Cont)

LIST OF TABLES

SUMMARY

The objective of this program was to develop and test ceramic material systems for use in turbine blade tip seals at temperatures up to 1370°C. Two concepts were studied to control blade wear:

1. Rub tolerant ceramic shroud liner materials

2. Ceramic blade-tip inserts

Each concept was studied separately and as part of a combined system.

In selecting materials several properties were considered to be of primary importance. These are:

1. Stability in an oxidizing atmosphere containing water vapor at temperatures up to 1538°C.

2. Resistance to thermal shock. A minimum of 1500 cycles between 370°C and 1538°C must be withstood without cracking or loss of material.

3. Impact resistance. Ballistic impact resistance on the exposed surfaces. This condition should be met for room temperature and service temperature.

4. Gas erosion. Erosion rates in combustion gases at Mach 0.9 for temperatures up to 1538°C should not exceed 0.025 mm in 200 hours. The combustion gases from liquid fuels will contain enough carbon particles to provide a typical erosive condition.

5. Dimensional stability to retain attachment integrity and, to a lesser extent, to maintain seal clearances.

Due to their superior properties for resisting thermal shock and oxidation two ceramics (silicon nitride and silicon carbide) in various forms were selected for the program. For the abradable shroud component, silicon nitride materials were tested in the sintered form at several densities, and in the honeycomb type structure in the reaction bonded form. Silicon carbide was tested primarily in the sintered form at several densities and particle sizes as compacts and in one honeycomb form with and without silicon impregnation. Hot-pressed silicon nitride and silicon carbide were also evaluated as blade tip inserts.

In overall performance, reaction bonded silicon nitride in fabricated structures (honeycomb) was a promising abradable at all temperatures up to 1370°C. The material abraded relatively uniformly and rub damage did not extend outside of the blade contact area. With sintered silicon nitride in compacted form at various densities, rub test results produced catastrophic

damage to the abradable material. Optimization of the silicon carbide abradable was not achieved. The best structure tested had a coarse grain size and generated debris that tended to erode adjacent areas by particle impingement.

Table A illustrates a comparison of performance of selected program materials. This table was prepared to give an overall analysis of the performance of the various material systems evaluated. The properties selected were believed to be those of greatest significance for selection of material systems for further development. Each material column is based on the best results of a class of materials. The values were assigned on the basis of materials that could be obtained during the program life and had the demonstrated capability of being fabricated into the required structure. Overall, silicon nitride honeycomb is considered to be superior to the silicon carbide materials. Late in the program vendors demonstrated significant advances in fabrication techniques of silicon carbide honeycomb. Table A is a brief summary of the relative merit of each material system.

Figure A shows the honeycomb configuration of reaction bonded silicon nitride abradable that performed most satisfactorily. In Figure B a typical silicon carbide compacted abradable is shown.

Table A

Relative Overall Merits of Systems Tested

Property	Ideal Value	Abradable Shroud Materials				Blade Tips	
		Compacted Silicon Nitride	Compacted Silicon Carbide	Honeycomb Silicon Nitride	Honeycomb Silicon Carbide	Silicon Nitride	Silicon Carbide
Thermal stability	10	7	8	9	8	10	10
Cost	5	3	5	2	4	3	4
Fabricability	7	2	7	4	5	7	7
Erosion resistance	10	1	5	10	7	10	10
Impact resistance	8	1	6	8	4	8	4
Reliability	10	2	8	9	7	10	6
NDT	10	4	7	9	8	8	8
Abradability	8	2	6	8	5	8	4
Engine ready	6	1	4	5	4	5	3
Long term benefits	8	2	7	7	7	8	5
Failure mode	10	1	8	10	5	8	5
Strength	9	3	6	7	6	9	5
Aerodynamic loss	10	10	9	5	5	8	8
Max. temperature	7	6	7	5	7	7	7
Total	108	45	93	98	82	100	88

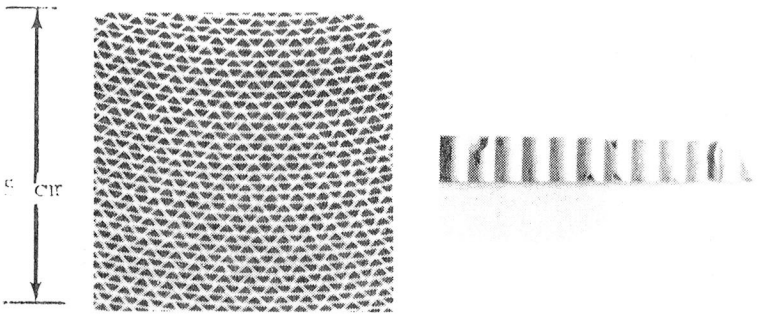

Figure A. Honeycomb Type Silicon Nitride

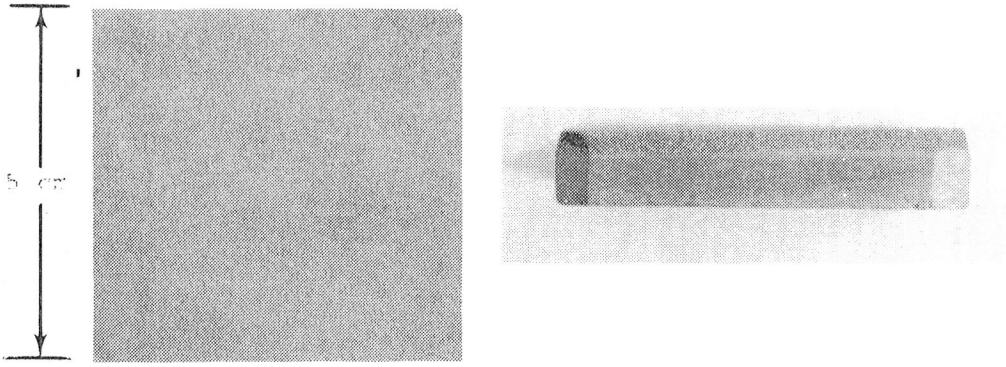

Figure B. Hot-Pressed Silicon Carbide Backing with an Abradable Silicon Carbide Face

Late in the program silicon carbide was fabricated into a 0.125 mm wall by 1.56 mm cell standard honeycomb configuration, Figure C. The material was tested as sintered and after silicon impregnation. Under typical rub conditions this configuration underwent catastrophic failure, indicating that either the configuration or material was less satisfactory than the reaction bonded silicon nitride in the 2 mm cell size configuration.

In evaluation of hot pressed silicon carbide and hot pressed silicon nitride blade tip inserts, rub tests indicated the superiority of the hot pressed silicon nitride. The latter material wore down slowly, similar to metals, but at one-sixth the rate. Hot pressed silicon carbide blade tips tended to fracture rather than wear.

A joining development was initiated during the program to bond the honeycomb type silicon nitride structure to a hot pressed silicon nitride backing. Pure silicon and silicon-titanium alloys were found to provide excellent bonds when processed in vacuum. Oxidation resistance of the bond zone was excellent up to 1200°C. Additional work in braze alloy development for these materials is needed to provide for wider gap brazing and, if needed, to bring the bond zone capability up to the 1370°C capability of the abradable material.

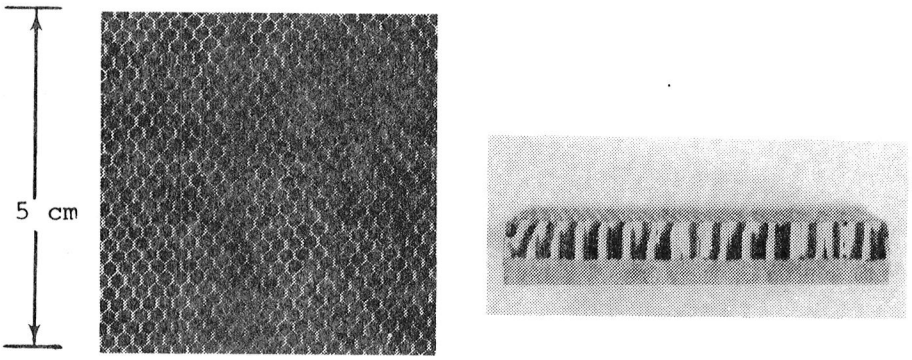

Figure C. Silicon Carbide Honeycomb Type Structure with an Integral Backing

This program is only a beginning of ceramic seal development. The effort has determined that reaction bonded silicon nitride structures have potential for development into a 1370°C abradable material. The material, cell size, and wall thickness need to be optimized followed by preliminary design and fabrication of tip shoes for both rig and engine testing.

Silicon carbide abradables also have a significant potential and probably an aerodynamic performance advantage. However, considerable development will also be required to optimize factors such as grain size, density, and fabrication techniques for joining them to a supporting structure.

Based on results of the tests and the design analyses performed in this program, additional silicon nitride ceramic tip insert testing should be performed. Ceramic tips offer a major advantage in reducing blade tip wear during rub.

1

INTRODUCTION

Gas turbine engines can develop significant power and efficiency losses in the hot sections due to leakage over the blade tips. This leakage can be minimized by using an abradable lining in the shroud to prevent blade wear when a rub occurs. Unless excessively large assembly clearances are used, blade tip rubs are inevitable due to thermal growth, engine deflections and eccentricity between the bladed disc and the shroud. Wear of the blade tip creates a 360-degree increase in the blade tip-shroud clearance while wear in the shroud occurs only in areas of interference and gives minimum tip leakage.

At low temperatures, less than 538°C, materials such as flame sprayed nickel-graphite can be used. However, as the operating temperature is increased, oxidation, corrosion and hot gas erosion become increasingly severe. At the present time, turbine temperatures of 1370°C are being considered for new designs. This temperature is above the operating limits of current production abradables for shroud liner materials unless large amounts of cooling air are used to reduce seal temperatures to an acceptable level. Several ceramics are not subject to these temperature limitations and are resistant to oxidation. This program evaluated commercially available silicon nitride and silicon carbide ceramic materials for use as turbine blade tips and for use as abradable shroud liners at 1370°C.

The following criteria were used during the program for selection of specific material systems for test:

1. Thermal stability up to 1370°C

2. Ready availability through current technology in a form suitable for incorporation into existing designs

3. Abradability for shroud liners or, conversely, high-strength and wear resistance for blade tips

4. Resistance to impact damage

5. Freedom from hot gas erosion in a gas turbine environment.

To determine the ability of a given material system to meet these criteria several laboratory tests were conducted. These included burner rig, impact, furnace, and abradability testing. Abradability testing was conducted over a wide range of conditions to determine the effect of variations in rub conditions (i.e., temperature, velocity, interference rate) on system performance.

This report summarizes the experimental results and conclusions reached during this program.

2

TEST MATERIALS AND PROCEDURES

Consideration of ceramic materials was based on two primary requirements:

1. Low thermal expansion

2. Stability in an oxidizing environment.

Low expansion was considered to be one of the most important properties. Good thermal shock resistance is essential and a low coefficient of thermal expansion contributes to this property. Silicon nitride ($3.2 \times 10^{-6} °C^{-1}$) and silicon carbide ($4.3 \times 10^{-6} °C^{-1}$) are two of the lowest expansion ceramics available that are stable to 1370°C. Published data show good strength retention by these materials at temperatures of up to 1538°C. The hot-pressed structures have the highest strength values over this temperature span while reaction bonded silicon nitride (NC-350) and recrystallized silicon carbide have lower but consistent strength levels.

The experimental portion of this program was conducted with structures fabricated from silicon carbide and silicon nitride. In Figure 1 a flow chart is presented showing the overall structure of the test program.

The test program was designed to evaluate the effect of material type, structure and density in providing a useful 1370°C ceramic turbine blade tip seal materials system. The individual tests were selected to evaluate the primary characteristics that would affect performance, as follows:

1. Thermal and chemical stability in an oxidizing atmosphere at temperatures up to 1370°C

2. Resistance to thermal shock without cracking or loss of material

3. Rub tolerance with minimal blade wear

4. Impact resistance to prevent gross failure from foreign objects in the gas stream at temperatures up to 1370°C

5. Dimensional stability to retain attachment integrity and, to a lesser extent, to maintain seal clearance.

This section of the report details specific material systems evaluated and the test procedures used. Specific facility descriptions are presented in the Appendices.

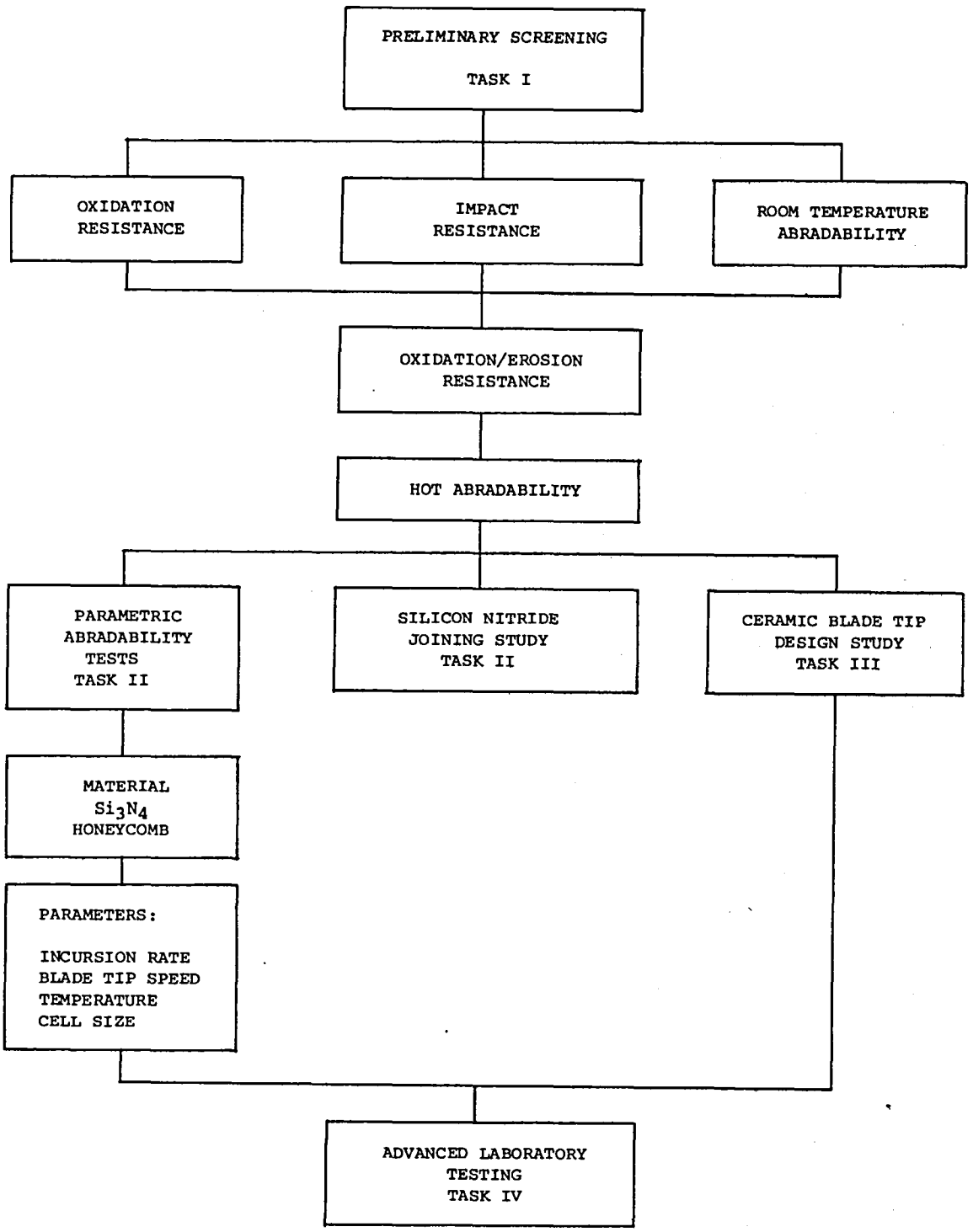

Figure 1. Flow Chart of Experimental Program

2.1 MATERIAL SELECTION

During the program materials were confined to those available from vendors without lengthy development programs. A total of 41 combinations, Table 1, were tested. These are described in this section. The first group of materials, 1 and 2, are fabricated by simultaneous wrapping of corrugated and smooth plasticized silicon nitride ribbons. After wrapping the structures are then sintered to provide the desired ceramic structure. A sketch of a representative specimen is shown in Figure 2. Photomicrographs of the structure can be found in the Results section of this report. The structure closely approximates that of the metal honeycomb used successfully at lower temperatures. Two cell sizes were obtained, as listed in Table 1.

The next two specimens (3 and 4) were fabricated using silicon nitride powder combined with silicon metal to fill the open cells. Sintering was conducted in a nitrogen atmosphere. Specimens 5 and 6 differed in that a high-temperature glass was used to bond the silicon nitride filler.

Low-density silicon nitride materials - systems 7, 8 and 9 were fabricated by reaction bonding with target densities of 60, 50 and 40 percent of theoretical density. The following three specimens, systems 10, 11 and 12, were made to the same specifications by a second supplier. Silicon carbide low-density structures fabricated from fine (-325 mesh) material were evaluated in systems 13 through 15. These structures closely paralleled the previously selected low-density silicon nitride specimens. The next material group was also fabricated from silicon carbide. However, systems 16, 17 and 18 differed from previous structures in that a relatively coarse grain was used in their fabrication to reduce thermal shock sensitivity and improve abradability. Another silicon carbide structure was tested using 150 mesh grain as the starting point. This selection was made to decrease the particle size ejected during rub and subsequent downstream erosion by high-velocity particles.

Ceramic blade tips fabricated from silicon carbide and silicon nitride were compared in systems 22 and 23. A 60 percent dense silicon carbide material (system 16) was used as the abradable.

Systems 24 through 26 were composite structures, i.e., a low-density abradable combined with a high-strength backing. Previous samples did not include a backing and technique development was required to join them to a metal substructure.

In systems 27 and 28 ceramic tipped blades were tested in conjunction with 60 percent dense silicon nitride. Similar tests were also conducted on an alternate grade of 60 percent dense silicon nitride in systems 29 and 30. Further blade tip tests were conducted on a honeycomb type silicon nitride (from systems 1 and 2) in systems 31, 32 and 33.

System 34 employed Bradelloy 500 as the shroud and a typical MAR-M421 blade tip. This abradable was included to provide a baseline in evaluating ceramic materials in this program.

Table 1

Material Systems

Material System Number	Seal Description			Blade Tip
1	Silicon nitride, honeycomb type	2 mm cell height		MAR-M421
2		1 mm cell height		
3	Silicon nitride, honeycomb type	2 mm cell height	Silicon powder fill and nitride	MAR-M421
4		1 mm cell height		
5	System 1	Filled with glass bonded silicon nitride		MAR-M421
6	System 2			
7	Reaction bonded silicon nitride	60 percent dense	Vendor "A"	MAR-M421
8		50 percent dense		
9		40 percent dense		
10	Reaction bonded silicon nitride	60 percent dense	Vendor "B"	MAR-M421
11		50 percent dense		
12		40 percent dense		
13	Silicon carbide 320 mesh	60 percent dense		MAR-M421
14		50 percent dense		
15		40 percent dense		
16	Silicon carbide 100/60 mesh	60 percent dense		MAR-M421
17		50 percent dense		
18		40 percent dense		
19	Silicon carbide 150 mesh	60 percent dense		MAR-M421
20		50 percent dense		
21		40 percent dense		
22	Silicon carbide 100/60 mesh	60 percent dense		Silicon nitride
23		60 percent dense		Silicon carbide
24	Silicon carbide graded abradable to high density backing		High density	MAR-M421
25			Medium density	
26			Low density	
27	Silicon nitride 100-150 mesh			MAR-M421
28	Reaction bonded	60 percent dense		Ceramic tip
29	Silicon nitride sintered	60 percent dense		MAR-M421
30		60 percent dense		Ceramic tip
31	Corrugated silicon nitride	2 mm cell height		Thin MAR-M421 tip
32		2 mm cell height		Ceramic tip
33		1 mm cell height		Ceramic tip
34	Bradelloy 500		Baseline	MAR-M421
35	Silicon carbide 1/16 cell honeycomb			MAR-M421
36	Silicon carbide 1/16 cell honeycomb, siliconized			MAR-M421
37	Silicon nitride	50 percent dense	Vendor "C"	MAR-M421
38		60 percent dense		
39	Silicon carbide foam	40 percent dense		MAR-M421
40		50 percent dense		
41		60 percent dense		

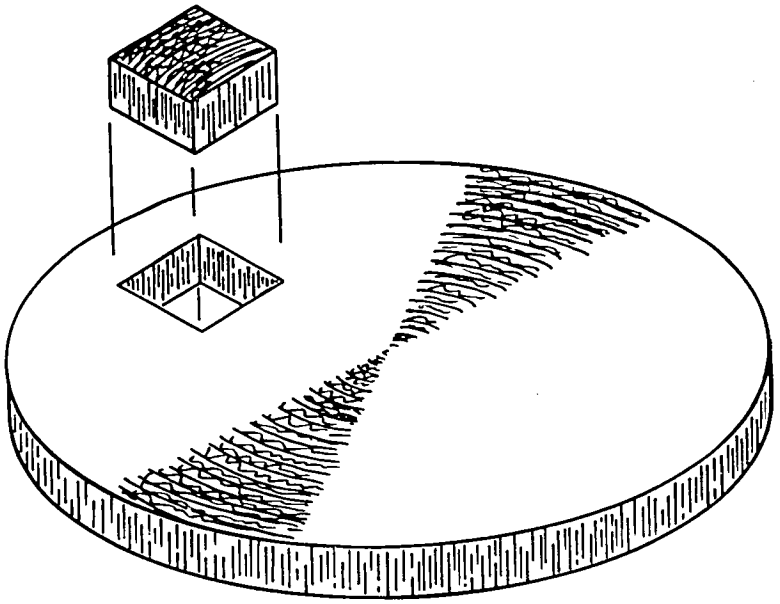

Figure 2.

Wound Structure of Reaction Sintered Silicon Nitride Showing Location of a Typical Test Specimen (No Scale)

Systems 35 and 36 were produced specifically for this program. Using standard 1/16 cell Hastelloy X honeycomb as a pattern, the supplier duplicated the honeycomb structure with an integral silicon carbide backing.

Systems 37 and 38 were obtained from a third silicon nitride source. This addition was made to determine if changes in fabrication technique would enhance performance.

The final group, systems 39 through 41, were foamed silicon carbide. This approach was tested as an alternate to the sintered structures of comparable density tested earlier in the program.

All of the abradable test specimens were obtained in a size 50 x 50 x 6.4 mm. Ceramic blade tips were fabricated from hot-pressed silicon carbide and silicon nitride. The test blade tips were equilateral triangles 0.31 cm on a side in cross-section by 2.5 cm long. The corners were slightly rounded to control edge chipping. A modified turbine blade from a Solar Centaur engine was used in the abradability testing. This blade is shown in Appendix A.

2.1.1 Oxidation Resistance

Samples, 25 x 25 x 5 mm, were weighed, measured and placed in an electric furnace preheated to 1370°C with static air as the atmospheric environment. After 50 hours exposure the samples were removed from the furnace, cooled to room temperature, and weighed. They were then returned to the furnace for an additional 50 hours exposure. The cycle was then repeated every 100 hours until a total of 500 hours exposure was reached. At completion of the test, weight change data was evaluated and extrapolated to indicate the probable results of a 10,000-hour exposure.

In addition, the samples were examined visually for cracking, warping or other evidence of failure each time they were removed from the furnace. Sections were prepared of each material for metallographic examination after 500 hours exposure and compared with samples taken from each material prior to test.

2.1.2 Ballistic Impact

The test materials were evaluated for ballistic impact resistance as follows. Each specimen was adhesively bonded to a steel backing and then placed in the ballistic impact test facility (App. B) to give an impact angle of 30 degrees. The equipment was standardized at an impact velocity of 127 mps using a steel ball 4.78 mm in diameter with a mass of 0.440 gms. After test the specimens were examined for impact damage (typically cracking, material loss) and the systems ability to withstand foreign object impact during engine operation.

2.1.3 Abradability

Abradability of the materials was initially performed at room temperature. Samples of each composition (50 x 50 x 5 mm) were adhesively bonded to a steel support fixture and machined to a 21.6 cm radius. Both grinding and single-point machining were used. The single-point machining proved to be the most effective with these materials. Solar turbine blades fabricated from MAR-M421 alloy were used in the turbine disc for these abradability tests. These blades were mounted in the disc and radius ground to a length of 6.4 mm for windage control.

During test, the sample temperature rise (monitored by a thermocouple located 1.3 mm beneath the initial center of rub) was automtically recorded. After testing, blade wear was measured and the appearance of the tip observed. Wear and relevant changes in the abradable materials were also determined.

Representative specimens were prepared from both the blades and abradable test specimens for metallurgical examination. From these data overall rub performance was evaluated for the material under test.

The baseline abradability test parameters were as follows:

- Temperature: ambient (82°C due to air friction)
- Blade velocity: 427 mps
- Ingression rate: 0.025 mm per second
- Depth of rub: 0.76 mm

Further evaluation of abradable seal material systems was performed at elevated temperatures on the rub test rig. These tests are similar to those conducted at room temperature except that the sample temperature was stabilized at 1370°C prior to test. Metallurgical sections were prepared after test to detect any changes in the material resulting from the test.

A detailed description of this test facility can be found in Appendix A together with a sketch of a typical test specimen.

2.1.4 Hot Gas Erosion

When oxidation, abradability, and ballistic impact tests were completed, the most promising systems were then tested at elevated (1370°C) temperatures for hot gas erosion.

Hot Gas Erosion Tests

The test facility was operated with kerosene fuel and preheated air. Combustion products at a velocity of 550 mps was directed onto the sample at an impingement angle of 30 degrees to the sample surface. During test the sample surface temperature was monitored optically and the burner adjusted to maintain it at 1370°C. Additional data was obtained by thermocouples located 6.4 mm beneath the initial sample surface. This temperature data was used to maintain reproducible test conditions.

After testing for 100 hours, sample weight change, the depth of the erosion, and the area over which the sample was eroded was measured. The relative erosion characteristics were recorded for each material.

Appendix C provides a description of the hot gas erosion test facility.

2.1.5 Compressive Strength

The silicon nitride honeycomb was selected as the material most nearly approaching the requirements for a ceramic blade tip seal. Compressive strength measurements were conducted on this material.

The compressive tests were performed using a cylindrical alumina loading block. The alumina cylinder was cut with a diamond wheel and finished with abrasive paper to insure that loading surfaces were parallel. The cylinder was 6.4 mm long with an O.D. of 7.8 mm and an I.D. of 5.0 mm. The ring configuration was selected to reduce the required load at failure to a value within the limits of the testing equipment while still covering a representative area of the specimen. The loading area calculated from these dimensions was 28.6 mm^2.

Prior to test the silicon nitride honeycomb was imbedded in wax and cut into 25 x 25 x 6.2 mm test pieces. The wax was then melted out and the honeycomb brazed to a hot-pressed siicon nitride backing for testing. Thirty-two percent of the bulk surface area (A) of the honeycomb was ceramic and the remainder voids. Ribbon area was determined as follows:

$$A_{Ribbon} = 0.32\ A_{Bulk} = 9.2\ mm^2$$

Compressive stresses were calculated based on the ribbon loading area:

$$\sigma_c = \frac{\text{Failure load}}{A_{Ribbon}}$$

where σ_c = axial compressive stress

Figure 3 illustrates the loading geometry. The blackened areas represent the compressive loading area.

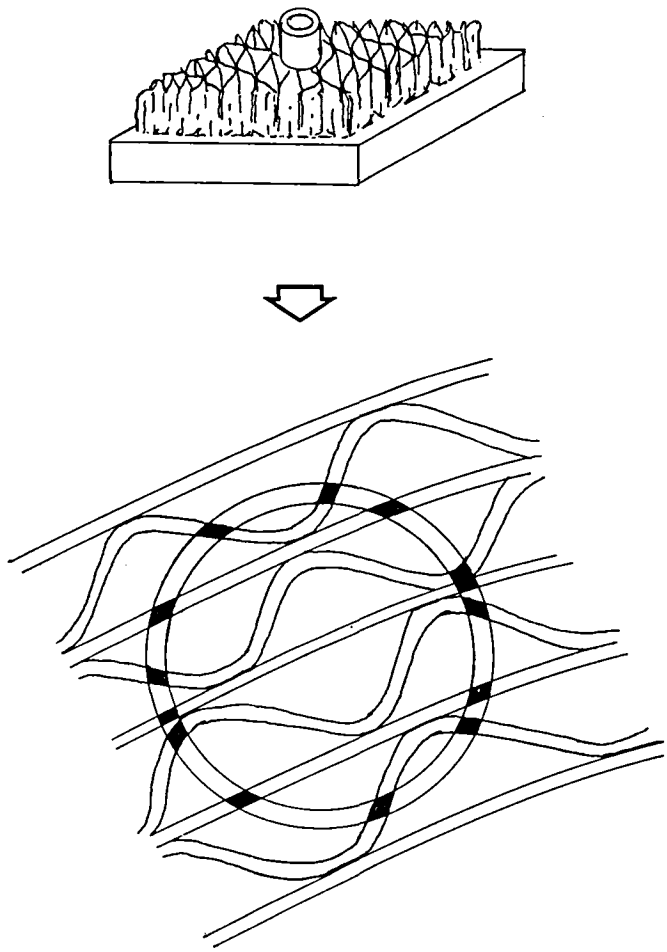

Figure 3.

Loading Geometry for Compression Tests

2.1.6 Modulus of Rupture

The modulus of rupture was also determined for silicon nitride honeycomb. Three-point bending tests were performed. Samples were cut to size while encased in wax. Braze alloy was then introduced into the nodal areas to simulate the as-brazed condition. Stress values were calculated based on bulk dimensions. The honeycomb sample was oriented so that the ceramic ribbon was approximately 45 degrees to an axis running lengthwise. This orientation was selected as a compromise representative of the overall structure. Temperature was varied over the range of ambient to 1427°C. The test arrangement is shown in Figure 4.

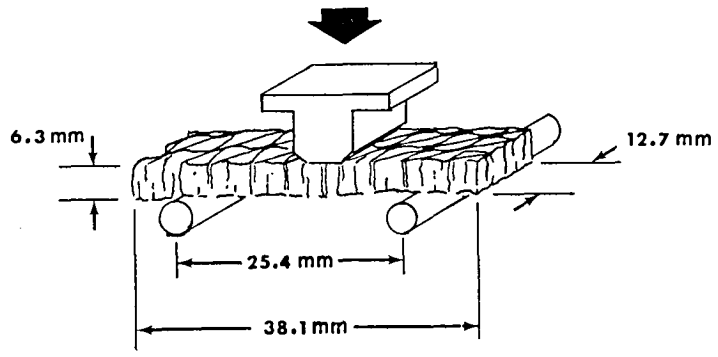

Figure 4. Three-Point Bending Test of Silicon Nitride Honeycomb

The modulus of rupture was calculated using the flexure formula:

$$\sigma_R = \frac{Mc}{I}$$

where σ_R = modulus of rupture

M = bending moment

c = distance from centroidal axis to outerrmost fiber

I = moment of inertia.

3

EXPERIMENTAL RESULTS

As the program progressed, materials and test procedures were adjusted to benefit from experimental data. Over 100 different specimens were received during this program as variations of the low-density and ribbon structures made from silicon carbide and silicon nitride. These are reported in groups since variations within a type were relatively minor. Where exceptions occur these are noted.

The following sections detail results of the test program.

3.1 CHARACTERIZATION OF MATERIALS

Upon receipt, each test material was weighed and measured. This data was used to calculate its apparent density. Metallurgical sections were also prepared to establish its initial structure for evaluation at this time and determination of changes occurring during test. Results of the density calculations are reported in Table 2. The systems with which each material is associated can be identified by reference to Table 1. The value of 3.44 gm/cc for silicon nitride (Handbook of Chemistry and Physics, 49th edition) was used as the basis for calculating relative densities. For comparison purposes only, the silicon nitride honeycomb structures (Fig. 5) were treated as a homogeneous structure. Subsequent measurements showed the reaction bonded ribbon used in their manufacture had a density of 80 percent (2.8 gm/cc) of the literature value. Filling the openings increased its bulk average density to 33 percent (1.14 gm/cc) of theoretical density. Silicon carbide materials very closely approached specified values. These were based on a theoretical density of 3.217 gms/cc (ibid). Two types were received initially, as indicated in Table 2. The first was manufactured from a -325 mesh powder and the second from a combination of -100 and -60 mesh material. The -325 mesh materials were less uniform in structure than their coarse grained counterparts. Evidence of high- and low-density areas was observed as striations in the material. The coarser grained structure was uniform in appearance. A typical low-density silicon carbide material is shown in Figure 6.

Foamed silicon carbide materials were also obtained as illustrated in Figure 7. These materials exhibited wide pore size variations, as is evident in the photograph. The structures were also friable and difficult to handle.

Table 2

Average Bulk Density of Ceramic Abradables

Material System(s)*	Material	Density (gms/cc)	Percent Theoretical Density	
			Specified	Actual
3 and 6	Corrugated Silicon Nitride 1 mm Cell Size	0.823	None	23.9
2 and 5	Corrugated Silicon Nitride 2 mm Cell Size	0.697	None	20.3
25, 26 & 27	Hot Pressed Silicon Carbide	3.22	100	100
22 and 25	Silicon Carbide 100/60 Grit	2.00	60	62.2
23 and 26	Silicon Carbide 100/60 Grit	1.60	50	49.7
24 and 27	Silicon Carbide 100/60 Grit	1.28	40	39.8
16	Silicon Carbide 320 Grit	1.99	60	61.8
17	Silicon Carbide 320 Grit	1.64	50	51.0
18	Silicon Carbide 320 Grit	1.32	40	41.0
10 and 13	Silicon Nitride	2.18	60	63.4
12 and 15	Silicon Nitride	0.727	40	21.1
5	Filled Silicon Nitride (0.08) cell size)	1.11	None	32.3
6	Filled Silicon Nitride (0.04 cell size)	1.09	None	31.7
34	Silicon Nitride 100-150 grit (reaction bonded)	1.95	60	57.3
36	Sintered Silicon Nitride	2.25	60	66.6

*See Table 1

PAGE 15 MISSING IN ORIGINAL DOCUMENT.

PAGE 16 MISSING IN ORIGINAL DOCUMENT.

The results of these tests are shown graphically in Figures 9 and 10.

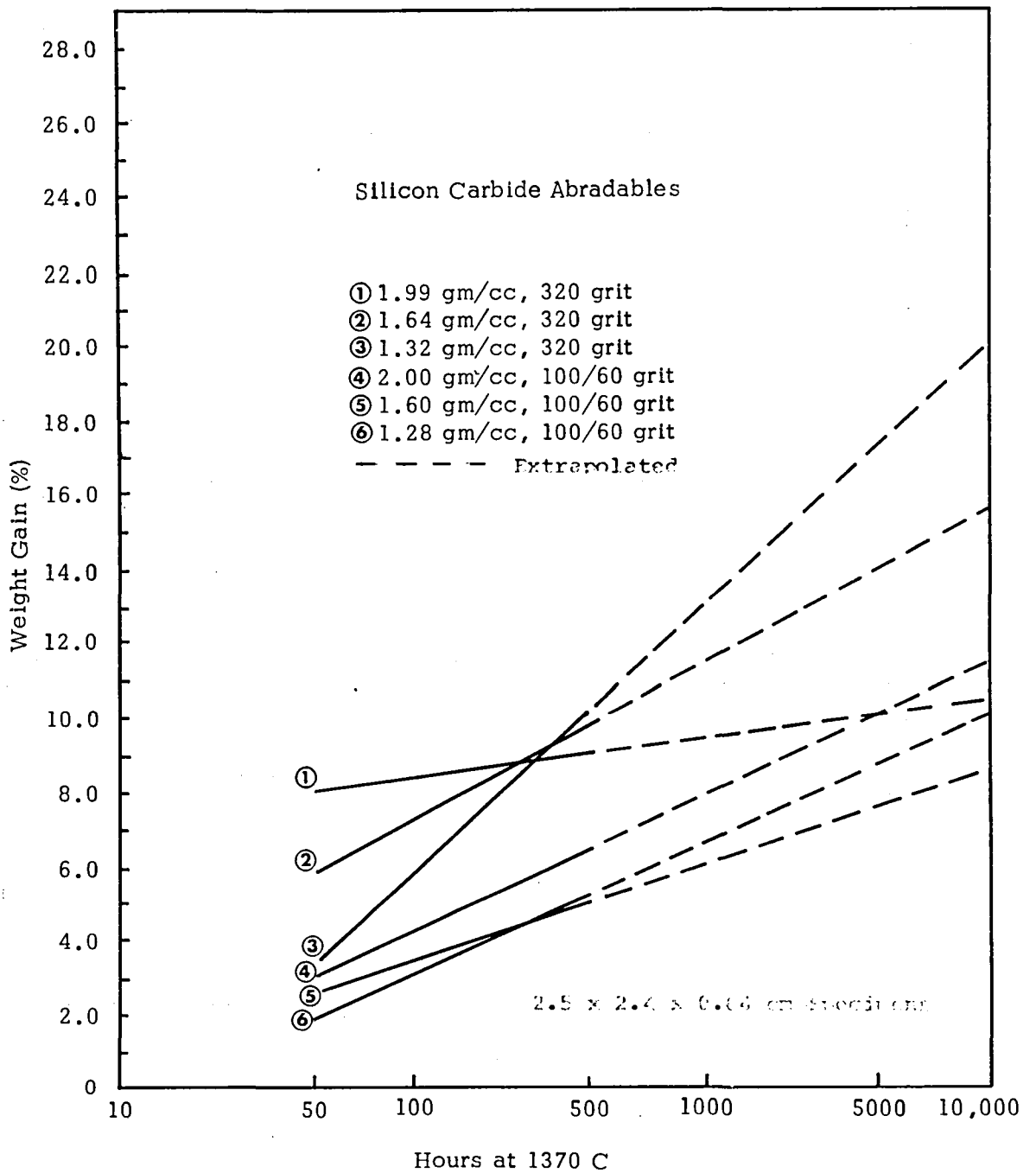

Figure 9. Effect of Elevated-Temperature Testing on Low-Density Silicon Carbide Abradables

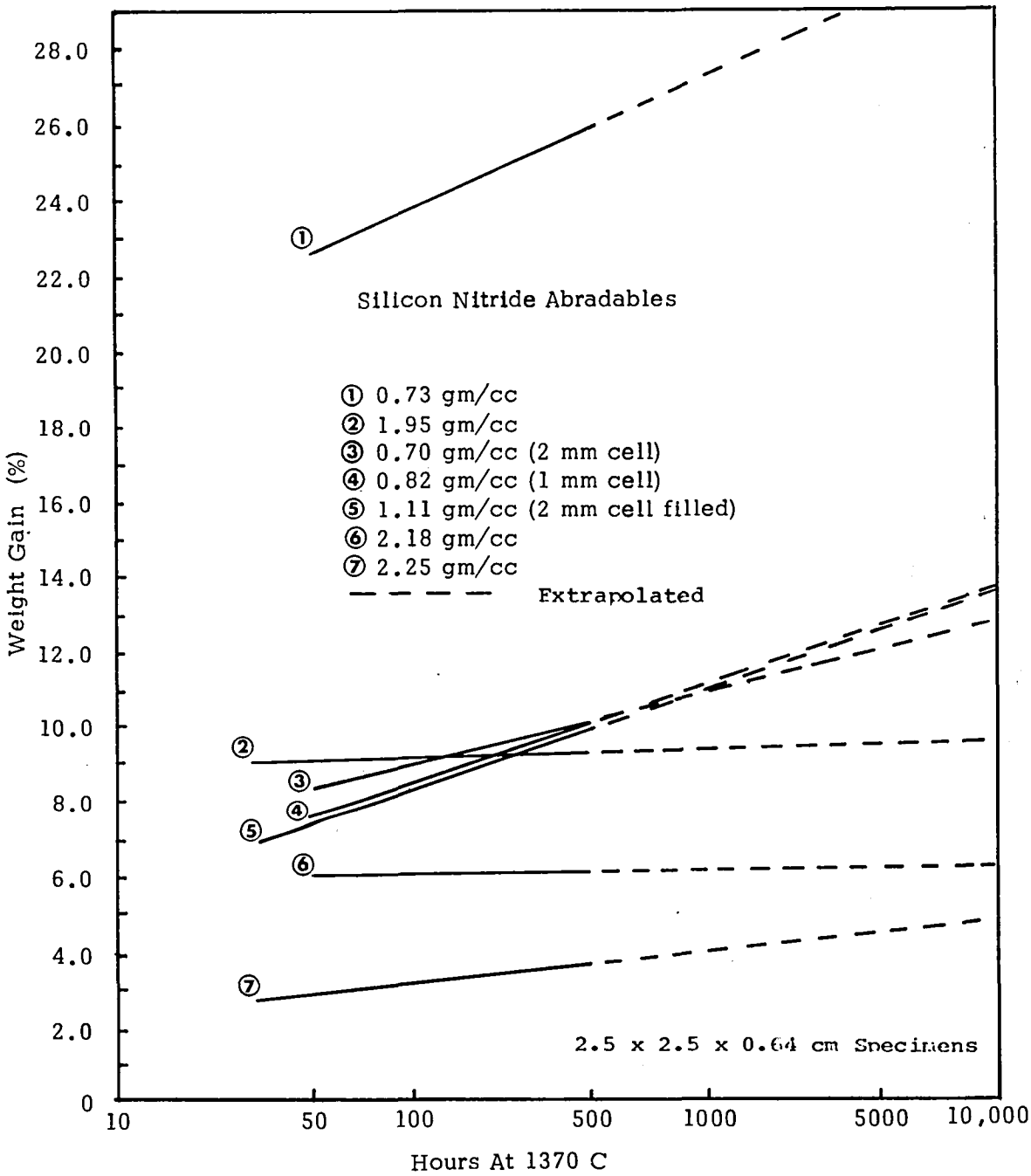

Figure 10. Effect of Elevated-Temperature Oxidation Testing on Low-Density Silicon Nitride Abradables

A significant difference was observed in the response of silicon nitride and silicon carbide that related to basic composition rather than to the structure under test. The structures based on silicon nitride showed a rapid rate of oxidation during the first 50 hours of test. This rate dropped to a low constant value for the remainder of the test.

It was also observed that as density decreased the rate of oxidation increased with a very rapid rate of oxidation occurring in the 20 percent dense material. In evaluating these test results, a value of 80 percent (the ribbon density - 2.8 gms/cc) should be used for the honeycomb silicon nitride structures. Hot-pressed silicon nitride samples showed very low weight gain when tested in this manner.

Photographs of filled and unfilled silicon nitride honeycomb samples before and after oxidation are shown in Figures 11 through 16. Both structures exhibited evidence of internal oxidation originating at surface imperfections and build up of glassy surface deposit during test. The filled specimens developed heavier surface deposits which reduced the amount of internal oxidation. This deposit can be seen in Figures 15 and 16. The benefits obtained from reduced oxidation in the filled structures were offset by the mechanical failure in the nodal areas. Numerous cracks developed in the silicon nitride ribbon. These appeared to originate in areas of heavy surface deposits and at acute angles in the joint area. The filled structures also exhibited a migration of the glass used to retain the silicon nitride phase. The binder concentrated on the exposed surface as well as the silicon nitride core. The unfilled silicon nitride structures were relatively free of mechanical failures resulting from the oxidation testing.

In contrast to the silicon nitride materials, structures based on silicon carbide had a nearly constant rate of oxidation during the test. The fine grained, low-density samples showed the least stability during test. Coarse grained samples (100/60 mesh) were less affected, particularly in the 60 percent dense material. The fully dense blade tips were little affected by exposure in air at 1370°C and no significant changes were detected as a result of the test. Generally, the oxidation rate was proportional to the relative surface area of the sample.

Bradelloy 500 was also subjected to a 1370°C oxidation test. After two hours, the Hastelloy X honeycomb had deteriorated to the point where the physical integrity of the sample was lost (Fig. 17).

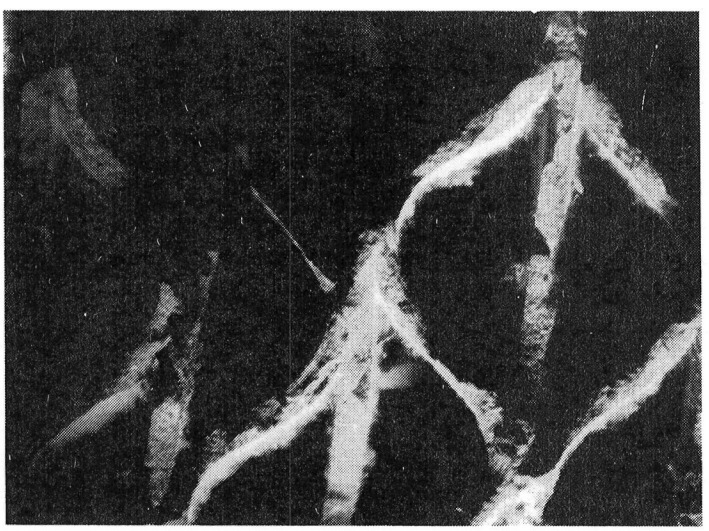

Figure 11.

2 mm Cell Unfilled Honeycomb Silicon Nitride Before Oxidation Test

Magnification: 16X

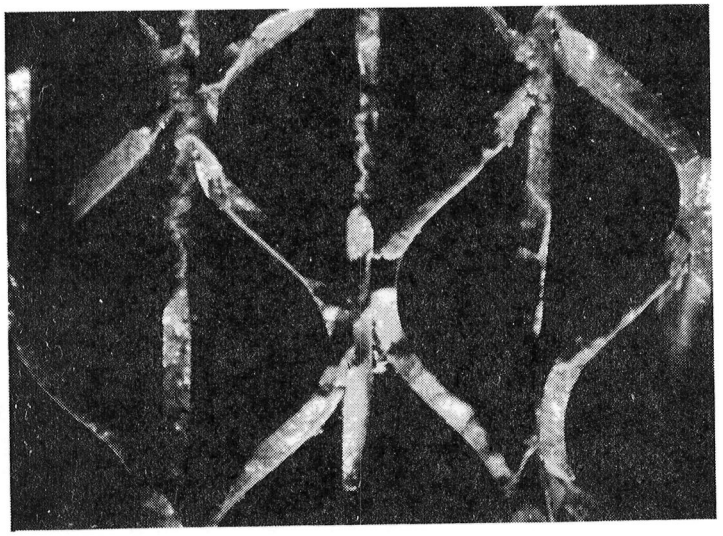

Figure 12.

2 mm Cell Unfilled Honeycomb Silicon Nitride After 500 Hours Oxidation Test at 1370°C

Magnification: 16X

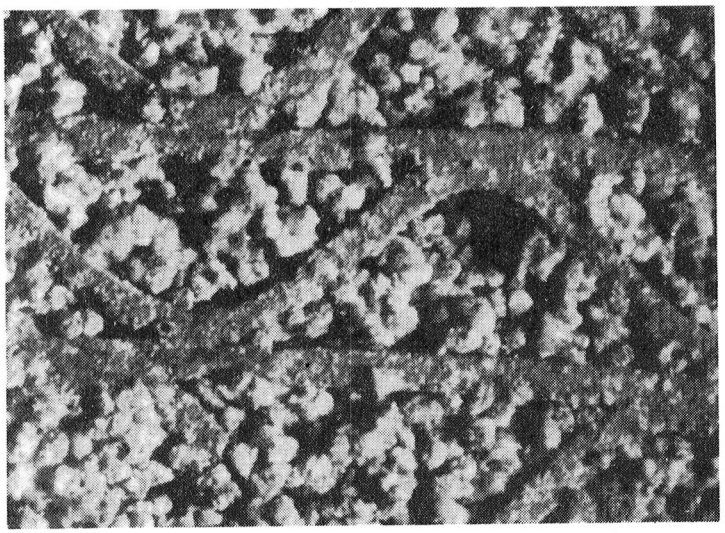

Figure 13.

2 mm Cell Filled Honeycomb Silicon Nitride Before Oxidation Test

Magnification: 24X

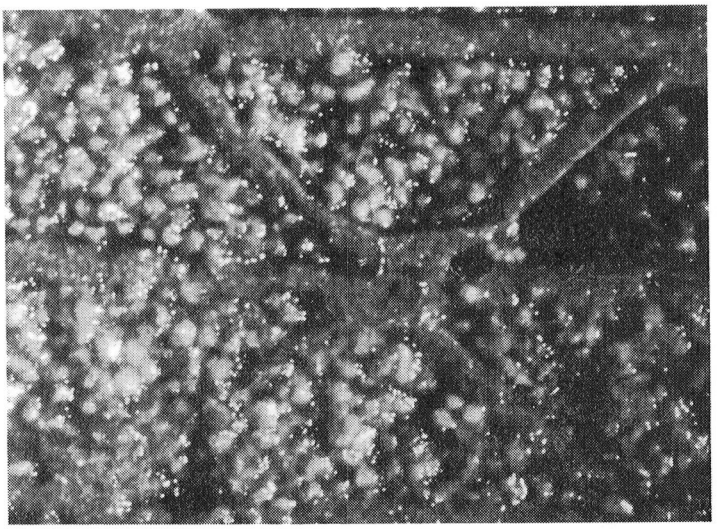

Figure 14.

2 mm Cell Filled Honeycomb Silicon Nitride After 500 Hours Oxidation at 1370°C

Magnification: 24X

Figure 15.

Nodal Joints of 2 mm Cell Filled Honeycomb Silicon Nitride After 500 Hours Oxidation at 1370°C

Magnification: 75X

(Arrows Indicate Oxide Penetration)

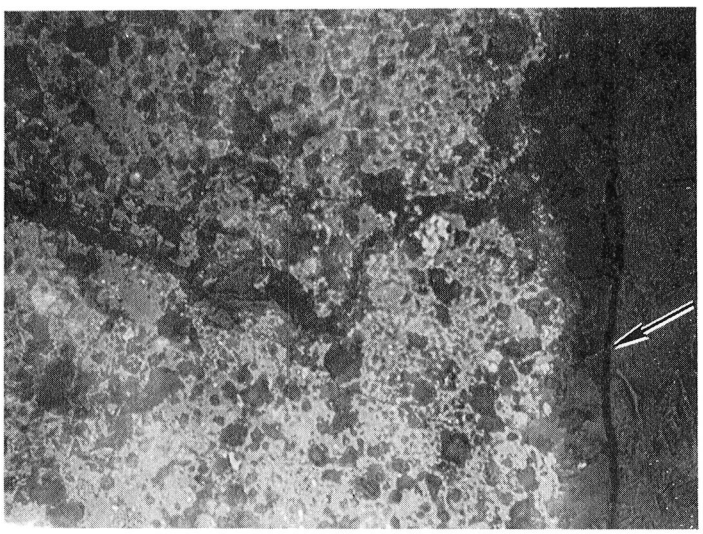

Figure 16.

Surface Layer Formed on 2 mm Cell Filled Honeycomb Silicon Nitride After 500 Hours Oxidation at 1370°C

Magnification: 500X

(Arrow Indicates Oxide Layer)

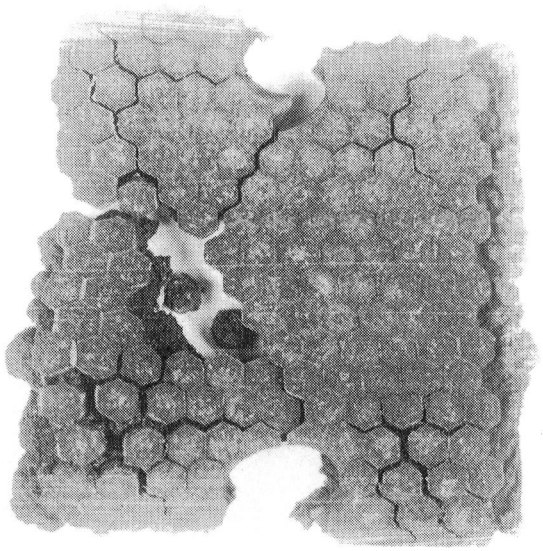

Figure 17.

Bradelloy 500 Specimen After Oxidation Test at 1370°C for 2 Hours

3.3 AMBIENT TEMPERATURE ABRADABILITY

The results of the abradability screening test conducted at ambient temperature of the material systems are summarized in Table 3. Because of the large number of tests, the data is abbreviated. In tests where the specimens failed no meaningful wear data could be obtained. The basic test conditions were:

Blade tip velocity	427 mps
Interference rate	0.025 mm/sec
Interference depth	0.76 mm
Temperature	ambient (82°C)

Two factors, grain size and density, were found to have the greatest effect on the performance of the silicon carbide low-density abradables. Three systems were tested fabricated from -325 mesh silicon carbide grain. These specimens differed in density (40-60% of theoretical). In rub tests all three failed mechanically. The specimens showed evidence of blade metal transfer (scabbing) to the abradable structure during the initial 10 to 20 seconds of rub. Considerable local heating of the contact surface was visible during test. During the last half of the test, the sample fractured. Figure 18 illustrates a typical test specimen. The fracture pattern and an area of heavy scabbing is visible. Use of a coarser silicon carbide grain size was more successful.

Samples fabricated from a nominal 50-50 mixture of 100 mesh and 60 mesh material showed improved properties. The coarser mesh specimens were somewhat weaker than the finer grained materials of equivalent densities. A 60 percent dense structure was found to give the best performance. A typical specimen, Figure 19, shows no indication of mechanical or thermal failure.

Blade wear was also low and the overall performance was good. However, the coarser particle (60 mesh) tended to erode adjacent areas when ejected at blade velocities. Three additional compositions were ordered. These were initially to be fabricated from 150 mesh material to reduce particle erosion and incorporated high-density silicon carbide backings for retention in the 1370°C testing. The vendor found that his current fabrication techniques were not compatible with these requirements and a change was made to accept 225 mesh material in the abradable structure. When tested for abradability, the samples failed after 20 seconds of rub.

A silicon carbide foam, 50 percent dense, was also tested for abradability. It was a fine grain material containing large voids (see Fig. 7). As with previous fine grained structures, the sample failed mechanically. Failure in this case was by complete loss of the specimen upon initial blade contact. Indications are that the specimens fractured at the bond line due to mechanical impact loading in shear rather than the thermal fracture observed in earlier tests.

Table 3

Room Temperature Abradable Rub Tests

Test Number	System Number (Table 1)	Abradable Material	Blade Material	Blade Wear	Comments
1	34	Bradelloy 500	MAR-M421	0.051 mm	Localized backing to honeycomb failure and hard surface glaze.
2	1	Silicon Nitride 2 mm cell	MAR-M421	0.025 mm	Red heat visible on contact. Blade shows heat coloration but no melting. Tip scored.
3	17	Silicon Carbide 50% dense 100/60 grit	MAR-M421	None	Sample delaminated and failed due to vibration and/or air blast prior to rub.
4	18	Silicon Carbide 40% dense 320 grit	MAR-M421	None measurable	Scoring on leading blades, others unmarked. Wear less than can be measured.
5	10	Reaction Bonded Silicon Nitride 60% dense	MAR-M421	None measurable	Sample rubbed smoothly first 5 seconds. At 6 seconds shear strain rapidly increased and sample shattered at 10 seconds total time.
6	14	Silicon Carbide 320 grit 50% dense	MAR-M421	None measurable	Smooth rub with some blade transfer to the abradable.
7	13	Silicon Carbide 320 grit 60% dense	MAR-M421	Slight scoring	Intermittent contact initially due to sample fracture. Complete breakup of sample after 15 secs.
8	16	Silicon Carbide 100/60 grit 60% dense	MAR-M421	Very light blade scoring	No blade damage but structure eroded in non-contact areas by high velocity particles from blade tip rub.
9	2	Silicon Nitride 1 mm cell	MAR-M421	No overall blade wear but scoring in nodes	Test sample exhibited more blade friction than 2 mm cell material. Light metal transfer (scabbing) also occurred.
10(2)	34	Bradelloy 500	MAR-M421	0.051 mm	Red heat visible. Smeared Hastelloy core. Penetrated 0.25 mm into specimen.
11(2)	34	Bradelloy 500	MAR-M421	0.025 mm	Incursion rate 0.013 mm second Sample came loose during test. Heavy glaze.
12(2)	34	Bradelloy 500	MAR-M421	Grooved - not measurable	Incursion rate 0.051 mm second Blade engaged evenly - red glow across surface.
13(2)	34	Bradelloy 500	MAR-M421	0.048 mm	Glazing produced non-uniform rub from local buildup of material
14(2)	34	Bradelloy 500	MAR-M421	0.066 mm	Penetration rate 0.013 mm seco Specimen eroded, blade loss high.
15	32	Silicon Nitride 2 mm cell	Hot Pressed Silicon Nitride	0.11 mm	Ceramic tip worn. No chipping evident. Tip to seal wear is 1 to 6.
16	32	Silicon Nitride 2 mm cell	Silicon Carbide	0.39 mm	Numerous fractures in ceramic tip. Tip to seal wear ratio 1 to 1.
17	23	Silicon Carbide 100/60 grit 60% dense	Silicon Carbide	0.19 mm	Tip fractures again evident.

(1) Standard test conditions: Tip speed - 427 mps, Incursion rate - 0.025 mm/sec, Interference depth - 0.76 mm.

(2) Baseline test series to evaluate reproducibility and effect of interference rate.

Table 3 (Cont)

Room Temperature Abradable Rub Tests

Test Number	System Number (Table 1)	Abradable Material	Blade Material	Blade Wear	Comments
18	7	Reaction Bonded Silicon Nitride	MAR-M421		Specimen shattered on contact.
19	29	Reaction Bonded Silicon Nitride (Sintered)	MAR-M421	0.15 mm	High surface heat generation during rub. Specimen cracked.
20	3	Silicon Nitride 2 mm cell Filled	MAR-M421	0.030 mm	Slight increase in blade wear. Filler lost during rub.
21	4	Silicon Nitride 2 mm cell Filled	MAR-M421	0.035 mm	Increased blade wear and scoring. Sample fractured during test.
22	11	Reaction Bonded Silicon Nitride 50% dense	MAR-M421	None	Sample failed on initiation of rub.
23	12	Reaction Bonded Silicon Nitride 40% dense	MAR-M421	None	Sample too soft. No blade wear but specimen eroded by high velocity gas and particles.
24	24	Silicon Carbide 40% dense	MAR-M421	None	Sample abraded early by heavily eroded gas stream.
25	29	Reacton Bonded Silicon Nitride 60% dense	Hot Pressed Silicon Nitride	(3)	Tip and specimen fractured during rub.
26	5	Filled Silicon Nitride Honeycomb	MAR-M421	(3)	Glass filler flowed to surface and was lost.
27	6	Filled Silicon Nitride Honeycomb	MAR-M421	(3)	Glass filler flowed to surface and was lost.
28	8	Reaction Bonded Silicon Nitride 50% dense	MAR-M421	(3)	Specimen fractured.
29	9	Reaction Bonded Silicon Nitride 40% dense	MAR-M421	(3)	Specimen eroded by high velocity gas.
30	11	Reaction Bonded Silicon Nitride 50% dense	MAR-M421	(3)	Specimen fractured.
31	12	Reaction Bonded Silicon Nitride 40% dense	MAR-M421	(3)	Specimen fractured.
32	15	Sintered Silicon Carbide 40% dense	MAR-M421	(3)	Specimen fractured.
33	19	Silicon Carbide 150 mesh 60% dense	MAR-M421	(3)	Specimen fractured.
34	20	Silicon Carbide 150 mesh 50% dense	MAR-M421	(3)	Specimen fractured.
35	21	Silicon Carbide 150 mesh 40% dense	MAR-M421	(3)	Specimen fractured.

(1) Standard test conditions: Tip speed - 427 mps, Incursion rate - 0.025 mm/sec, Interference depth - 0.76 mm

(2) Baseline tst series to evaluate reproducibility and effect of interference rate.

(3) Specimen failed. No meaningful measurement obtained.

Table 3 (Cont)

Room Temperature Abradable Rub Tests

Test Number	System Number (Table 1)	Abradable Material	Blade Material	Blade Wear	Comments
36	22	Silicon Carbide 100/60 mesh 60% dense	Silicon Nitride	0.05 mm	Good abrability with minimum tip wear. Some erosion adjacent to rub path.
37	24	Graded Silicon Carbide High density	MAR-M421	0.038 mm	Specimen fractured.
38	25	Graded Silicon Carbide Medium density	MAR-M421	0.019 mm	Specimen fractured.
39	26	Graded Silicon Carbide Low density	MAR-M421	(3)	Specimen fractured.
40	27	Sintered Silicon Nitride	MAR-M421	(3)	Specimen failed.
41	30	Reaction Bonded Silicon Nitride	Hot Pressed Silicon Nitride	(2)	Abradable fractured.
42	31	Silicon Nitride Corrugated	Special MAR-M421	0.60 mm	Squealer tip blade severely worn.
43	35	Silicon Carbide 1/16 Cell Honeycomb	MAR-M421	0.025 mm	Sample fractured after 20 secs rub.
44	36	Silicon Carbide 1/16 Cell Honeycomb, Siliconized	MAR-M421	0.25 mm	Sample fractured after 23 secs rub.
45	38	Reacton Bonded Silicon Nitride 60% dense	MAR-M421	(3)	Specimen fractured.
46	37	Reaction Bonded Silicon Nitride 50% dense	MAR-M421	(3)	Specimen fractured.
47	39	Silicon Carbide Foam, 40% dense	MAR-M421	0.10 mm	Specimen swept away during rub.
48	40	Silicon Carbide Foam, 50% dense	MAR-M421	(3)	Laminar shear of surface layer.
49	41	Silicon Carbide Foam, 60% dense	MAR-M421	(3)	Specimen abraded but high rate of gas erosion.

(1) Standard test conditions: Tip speed - 427 mps, Incursion rate - 0.025 mm/sec, Interference depth - 0.76 mm

(2) Baseline tst series to evaluate reproducibility and effect of interference rate.

(3) Specimen failed. No meaningful measurement obtained.

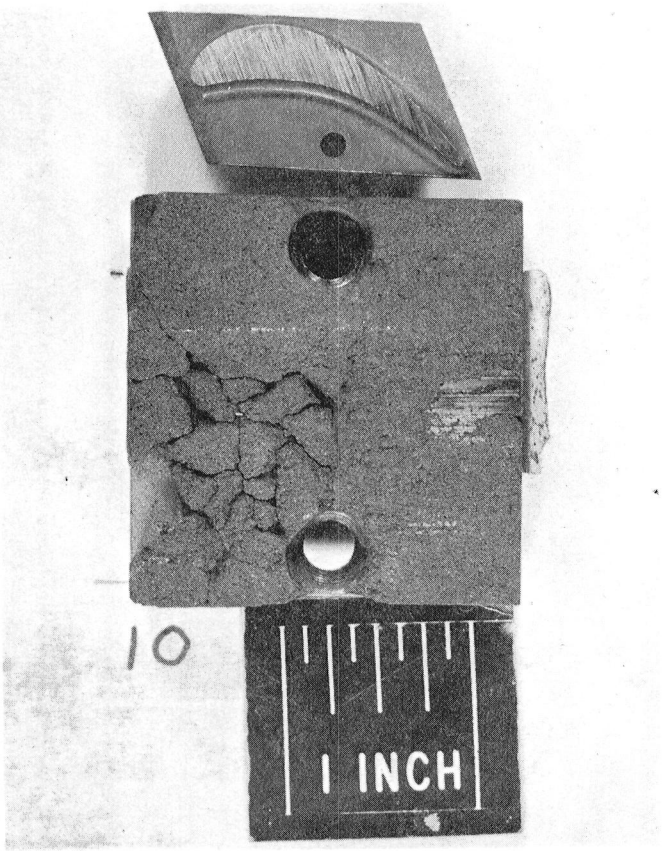

Figure 18.

Silicon Carbide, 50 Percent Dense, 320 Mesh, After Rub Test

Low-density silicon nitride materials were less successful than their silicon carbide counterparts. Material was obtained from three vendors; two fabricated by reaction bonding and one by sintering. The first vendor supplied 20 and 60 percent dense material which was processed by reaction bonding. The low-density (target value 40%) had insufficient strength to withstand initial blade contact. The specimens were completely destroyed during test due to their low strength.

The 60 percent dense reaction bonded silicon nitride material from all vendors failed in a similar manner. A typical specimen is shown in Figure 20. The sample exhibits scabbing and fracture with large areas lost completely. The sintered structure, Figure 21, exhibited little material loss. A single large crack was developed in the contact area. Heavy scabbing is evident and the specimen showed no evidence of the desired abradability.

The silicon nitride honeycomb structures exhibited many desirable characteristics during rub. A typical specimen is presented as Figure 22. The specimen shown has a 2 mm cell. The test results from the finer, 1 mm cell, structure were similar although some scabbing occurred with the latter material. This created higher blade wear.

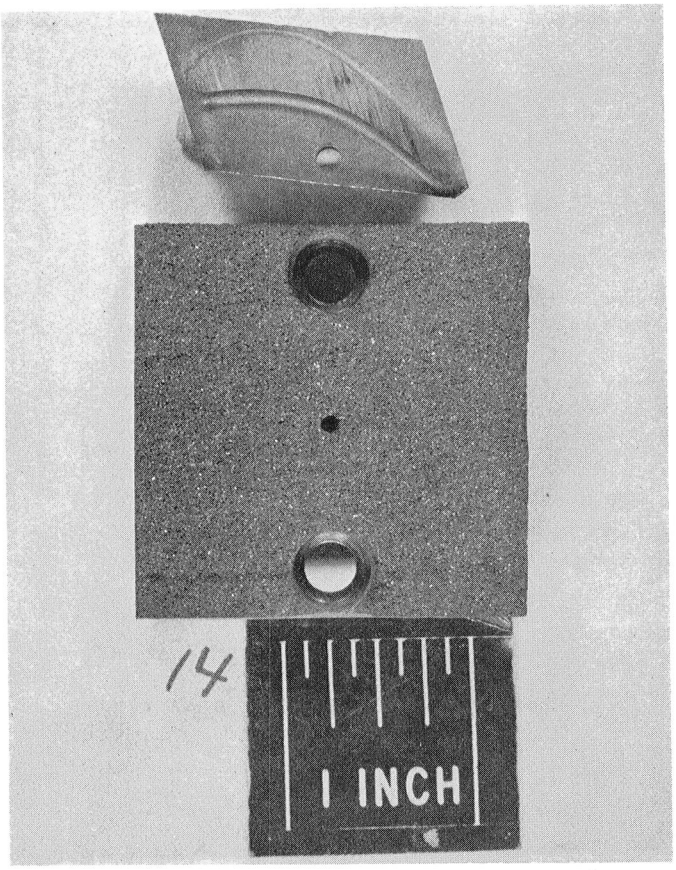

Figure 19.

Silicon Carbide, 60 Percent Dense, 100/60 Mesh, After Rub Testing

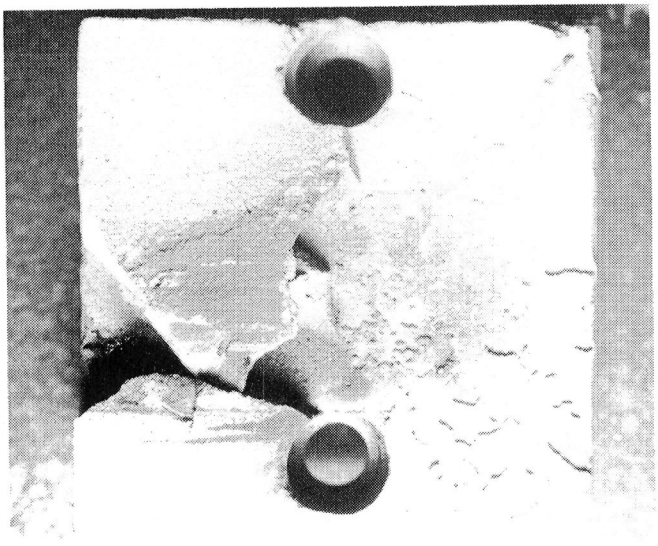

Figure 20.

Reaction Bonded, 60 Percent Dense, Silicon Nitride After Rub Test (Vendor A)

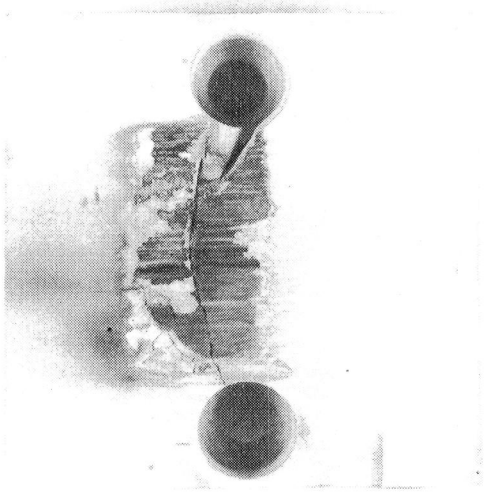

Figure 21.

Sintered, 60 Percent Dense, Silicon Nitride After Rub Test (Vendor C)

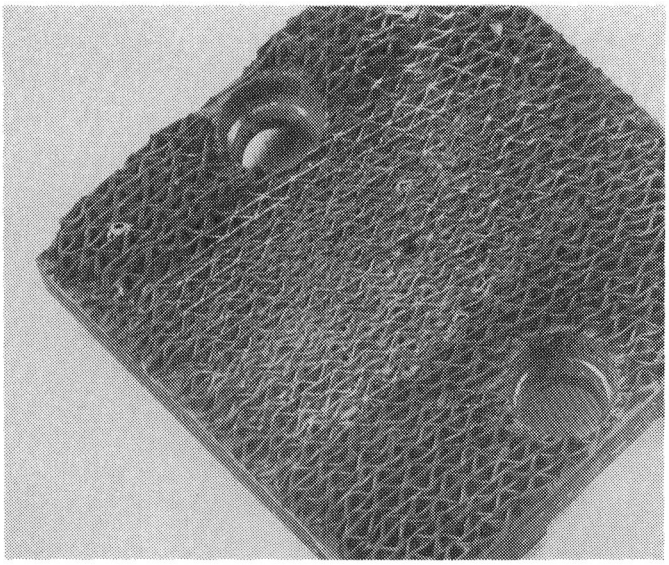

Figure 22.

2 mm Honeycomb Silicon Nitride After Rub Test

Honeycomb samples filled with glass bonded silicon nitride powder were also tested. Nitrided silicon bonded filled materials failed during processing. During the early stages of the rub some blade wear and heat generation were evident. The filler was lost as the test continued and the sample then behaved like the unfilled material. No measurable benefit was obtained from filling the honeycomb cells.

Ceramic tipped blades were tested and compared with a similar MAR-M421 configuration. One comparison between hot-pressed silicon nitride, hot-pressed silicon carbide and MAR-M421 alloy blade tips was made on 2 mm cell size silicon nitride honeycomb.

Figures 23 and 24 illustrate the appearance of a MAR-M421 turbine blade (reduced in the tip section to parallel the ceramic inserts) after rub. This test was conducted as a baseline for evaluting ceramic blade tips. The tip is worn for approximately 64 percent of the total penetration. Wear is over twice that of the ceramic tips from subsequent tests.

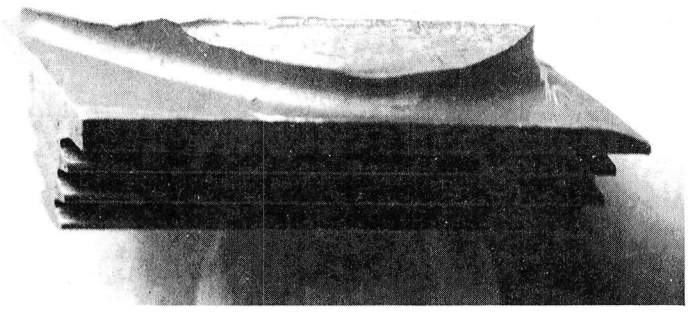

Figure 23.

MAR-M421 Blade Tip After Test Rub on Silicon Nitride Honeycomb

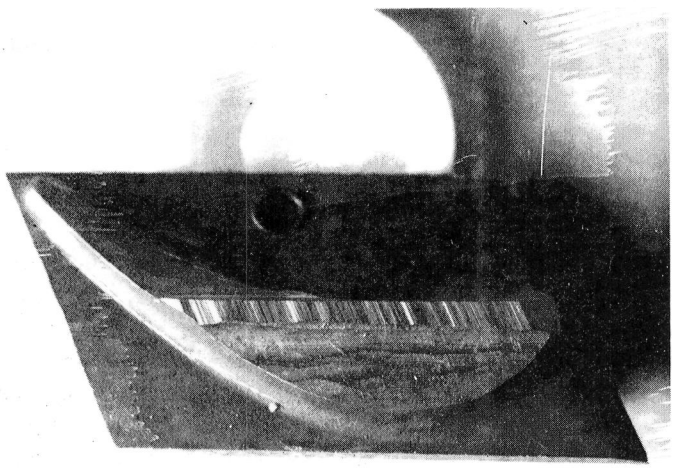

Figure 24.

End View of MAR-M421 Blade After Rub Test

Views are presented in Figures 25 and 26 of silicon nitride blade tips subjected to this test. The ceramic tipped blades were fabricated with small triangular inserts (3.1 mm per side) placed in eloxed dovetails using a standard test blade. During test the insert fractured in a plane perpendicular to the rub direction. Although not readily visible, small irregularities exist in the dovetail, creating point contact in some regions. The fracture appears to have originated at one of these high stress points. Very little edge chipping has occurred and the overall wear resembles a metal rather than a brittle ceramic material. The tip to seal wear of hot-pressed silicon nitride is approximately one-to-six in contrast to the two-to-one ratio of the metal tip tested previously.

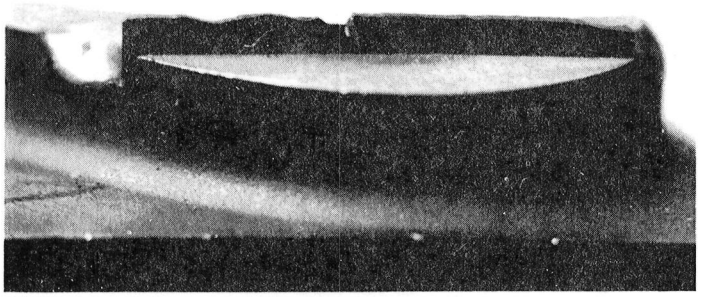

Figure 25.

Silicon Nitride Blade Tip Profile After Rub Test

Magnification: 2.75X

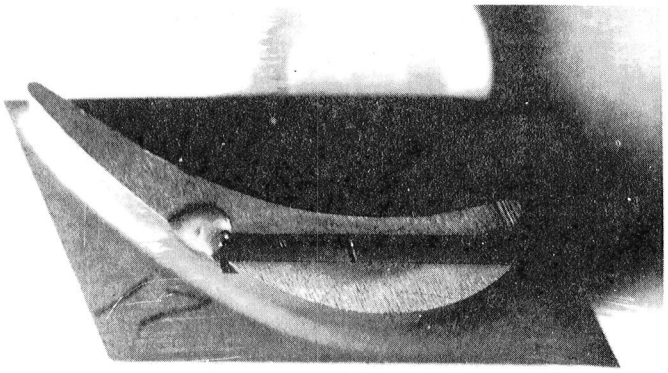

Figure 26.

Silicon Nitride Blade Tip After Rub Test

Magnification: 1.5X

Identical rub tests were also conducted with silicon carbide blade tips, as shown in Figures 27 and 28. Again, a single cross sectional fracture of the tips occurred during rub. Wear on this tip differed considerably from the silicon nitride test. The tip wear was exceedingly irregular. Numerous fractures occurred during rub with the subsequent loss of blade tip particles rather than the comparatively uniform continuous wear exhibited by the superalloy and silicon nitride tips. This tendency to fracture rather than wear is clearly evident in Figure 29, which is a higher magnification photograph of the silicon carbide blade tip. The local fracture planes and tendency to chip during rub is evident. Tip to seal wear ratio is approximately one to one, which is half that of the metal blade but six times the wear of the silicon nitride tip under similar test conditions.

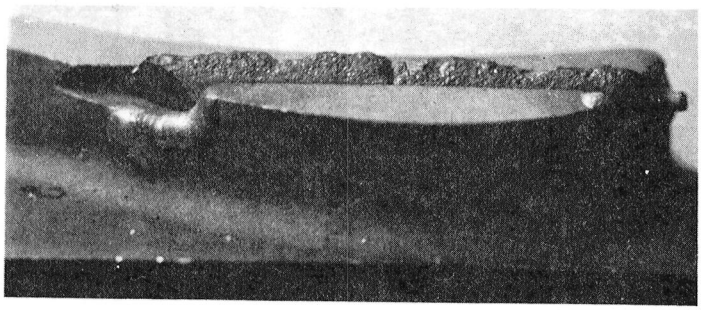

Figure 27.

Silicon Carbide Blade Tip After Rub Test on Silicon Nitride Honeycomb

Magnification: 3X

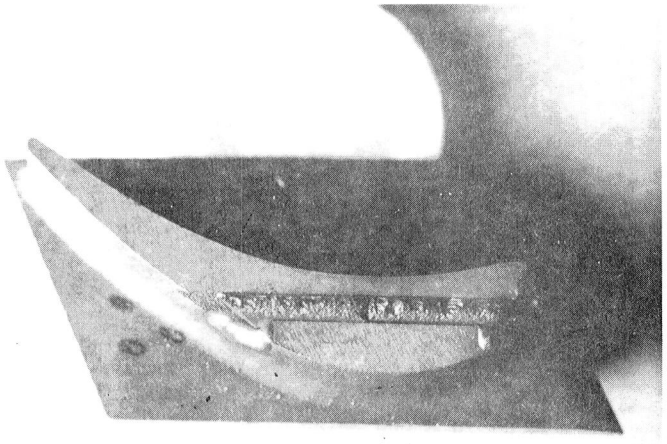

Figure 28.

Silicon Carbide Blade Tip After Rub Test on Silicon Nitride Honeycomb

Magnification: 3X

Figure 29.

Typical Section of a Silicon Carbide Blade Tip After Test

Magnification: 10X

Silicon carbide blade tips were also tested for wear characteristics using a 60 percent dense silicon carbide abradable. This abradable is of lower strength than the silicon nitride and, when tested with MAR-M421 blades, exhibits lower blade wear. As illustrated in Figures 30 and 31, the fracture previously observed when this tip was tested against the silicon nitride structure is evident. Tip wear against the low-density silicon carbide was about half the wear obtained when this tip material was tested on a silicon nitride structure, as previously reported.

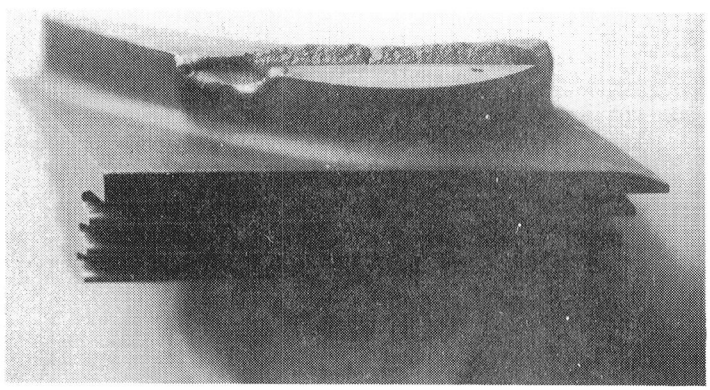

Figure 30.

Silicon Carbide Tip Profile After Rub on 60/100 Mesh Silicon Carbide, 60 Percent Dense

Magnification: 3X

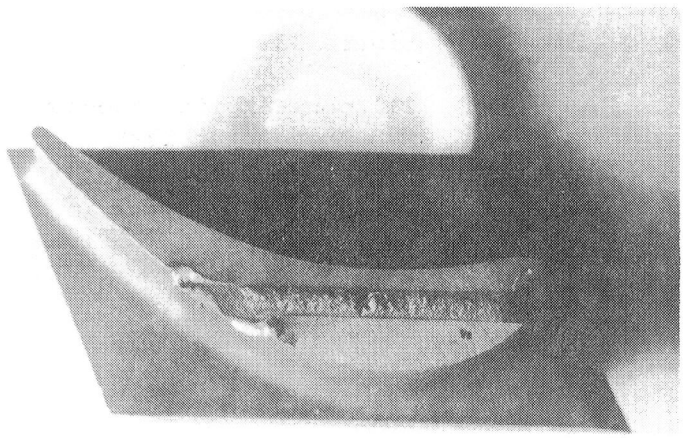

Figure 31.

Silicon Carbide Tip After Rub on 60/100 Mesh Silicon Carbide, 60 Percent Dense

Magnification: 3X

Two silicon carbide honeycomb structures were tested for abradability. The appearance of the unrubbed structure is shown in Figure 32. The accurate reproduction of the metal honeycomb pattern is evident. Voids between the adjacent cell walls existed in the metal core used as a pattern. The appearance of the specimens after test is shown in Figures 33 through 36. Both materials fractured after approximately 15 seconds of rub. They differed in that the siliconized material fractured above the backing, about 1.3 mm below the contact area. The unsiliconized material fractured at the base of the honeycomb structure or 2.5 mm below the contact point. Some blade scoring was evident in each test, but the brevity of the rub prevents significant wear evaluation.

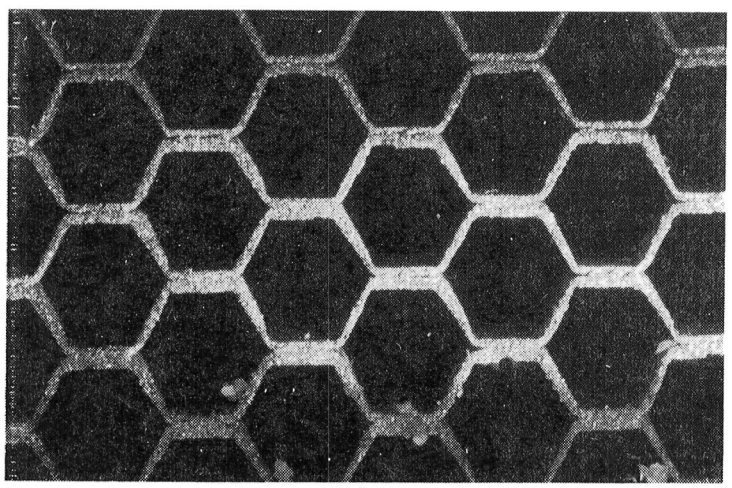

Figure 32.

Silicon Carbide Honeycomb Prior to Test

Magnification: 10X

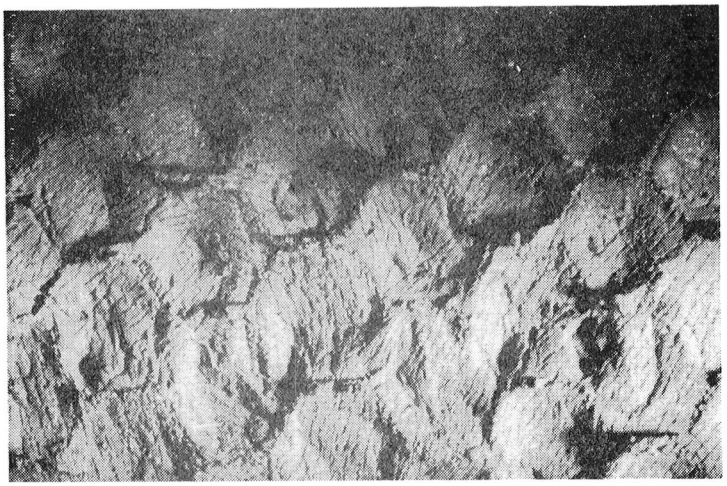

Figure 33.

Silicon Carbide Honeycomb
Rub Area After Test

Magnification: 10X

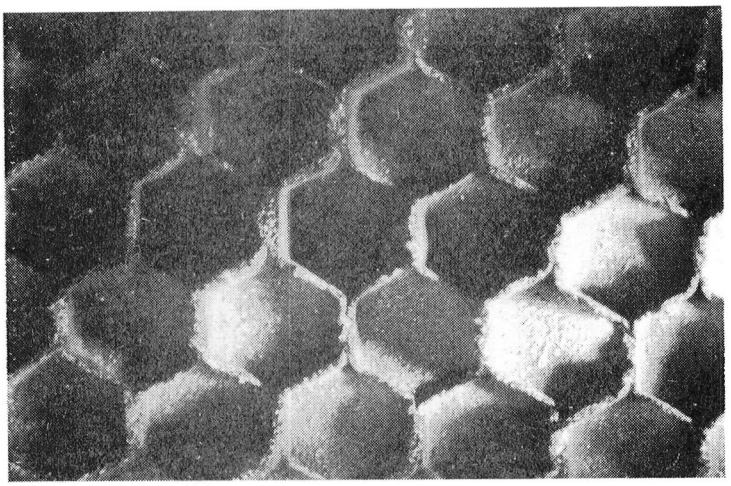

Figure 34.

Siliconized Silicon Carbide
Honeycomb Rub Area After
Test

Magnification: 10X

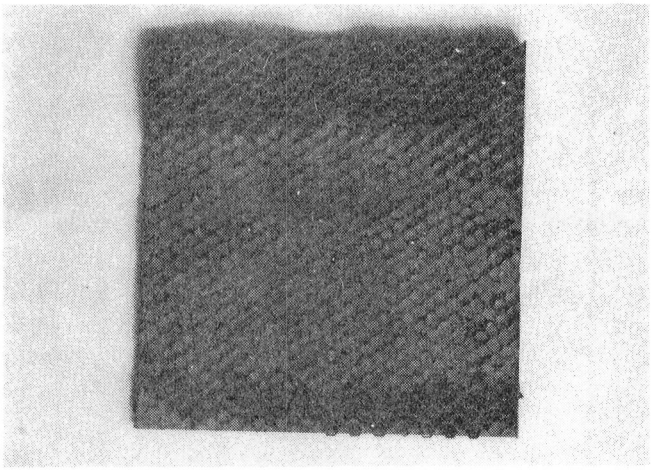

Figure 35.

Silicon Carbide Honeycomb
Specimen After Test

Magnification: 1X

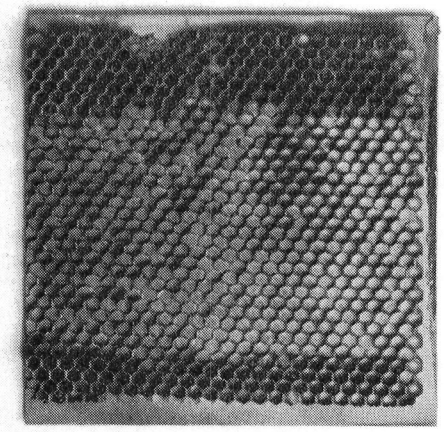

Figure 36.

Siliconized Silicon Carbide Honeycomb After Test

Magnification: 1X

As previously mentioned, Bradelloy 500 was selected as a baseline material. Considerable difficulty was encountered in establishing relevant baseline data on the Bradelloy 500 material. Under the standard test conditions at ambient temperature the material glazed, giving a hard wear-resistant surface and extremely high vibration levels in the test facility. Two test variations were tried with this material to further explain its behavior. These consisted of reducing the penetration rate to half the standard value (0.012 mm/sec) and in a second test the rate was doubled (0.050 mm/sec). Results of these tests are reported in Table 4 and are shown in Figures 37, 38 and 39. Increasing the penetration rate increased the sample temperature rate of rise. Shear force was uniform during this test and the high stress peaks encountered at the lower feed rates were eliminated. After test the high penetration rate sample was free of the glazing effects observed in the tests at lower penetration rates and a significant degree of abradability was demonstrated.

Table 4

Effect of Changing Ingression Rate on Rub Performance of Bradelloy 500 and MAR-M421 Turbine Blades

Ingression Rate (mm/sec)	Blade Wear (mm)	Bradelloy Temperature Rise (°C)	Abradable Appearance
0.013	0.066	167	No wear, heavy scabbing
0.025	0.048	200	Slight wear, followed by scabbing
0.051	None	278	Uniform removal
Tip velocity - 427 mps Interference - 0.76 mm Temperature - ambient			

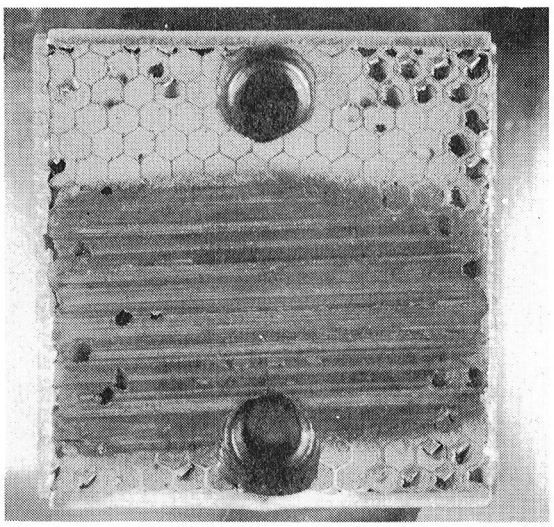

Figure 37.

Bradelloy Penetration Rate, 0.050 mm/sec

Magnification: 1X

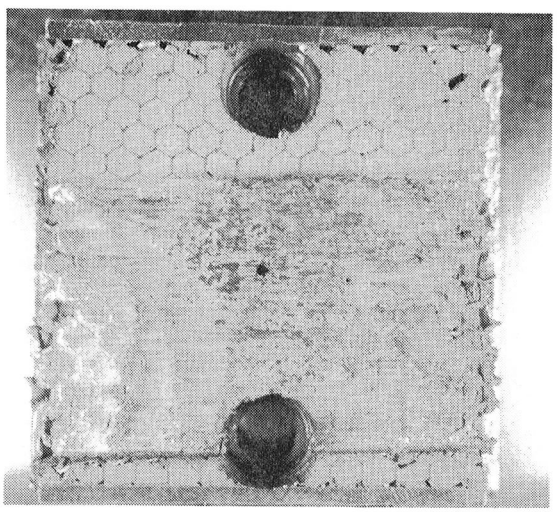

Figure 38.

Bradelloy Penetration Rate, 0.025 mm/sec

Magnification: 1X

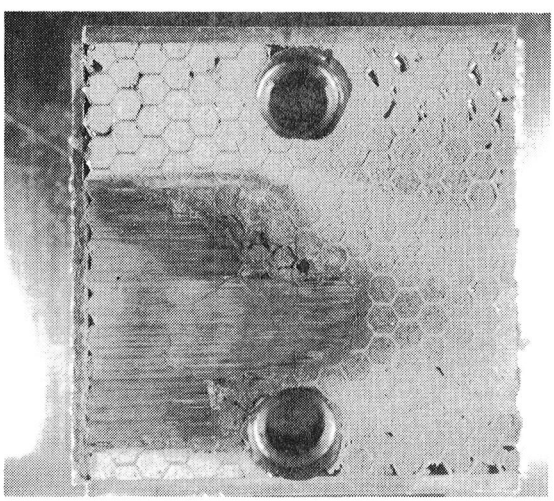

Figure 39.

Bradelloy Penetration Rate, 0.012 mm/sec

Magnification: 1X

3.4 ABRADABILITY TESTING AT 1370°C

Rub tests were conducted at 1370°C on low-density silicon carbide, unbacked silicon nitride honeycomb, filled silicon nitride honeycomb and brazed silicon nitride honeycomb. All failed to some degree during test limiting the data that could be obtained. A modified specimen holder, Figure 40, incorporating spring loading to minimize stresses due to differential thermal expansion and specimen variations was used for these tests. The results are summarized in Table 5.

The silicon carbide sample fractured and was lost during test. The blade tips were unmarked, except for slight evidence of debris impingement on the pressure face indicating failure occurred prior to a significant rub. No part of the specimen was recovered for post-test examination.

The silicon nitride honeycomb exhibited a clean fracture surface in the rub area. Portions of the specimen separated at the nodal joints allowing sections of the core to rise vertically into the blade tip path. This resulted in heavy rub in local areas. However, the material fractured cleanly and a uniform surface was evident at completion of the test. Blade wear was less than the accuracy of the measuring equipment and no signs of localized wear due to the sample movement was visible.

The fine, 1/32 cell, honeycomb fractured after approximately 20 seconds of rub. As with the silicon carbide specimen, no examination could be performed on this specimen. The blade tips were worn 0.38 mm indicating scabbing by the abradable since blade wear exceeded the amount of interference developed prior to specimen failure.

The filled honeycomb structure also failed during test. Some small pieces were found in the test cell. Examination of these indicated that the filler had migrated to the surface and was swept away by the blade tips. Insufficient debris was found to determine whether this occurred prior to or during rub or to establish the effect of the glassy phase on rub behavior.

A final test was conducted on 1/16 cell silicon nitride honeycomb core silicon brazed to a high-density silicon nitride backing. Examination after test revealed areas of braze failure during test. In these locations the core was completely lost. No correlation between material loss and rub pattern could be established.

Failure areas were found to be in sections where large gaps (0.25 mm or more) between the abradable and the backing occurred due to specimen irregularities. Some scabbing in the brazed nodal areas and associated blade grooving was also seen.

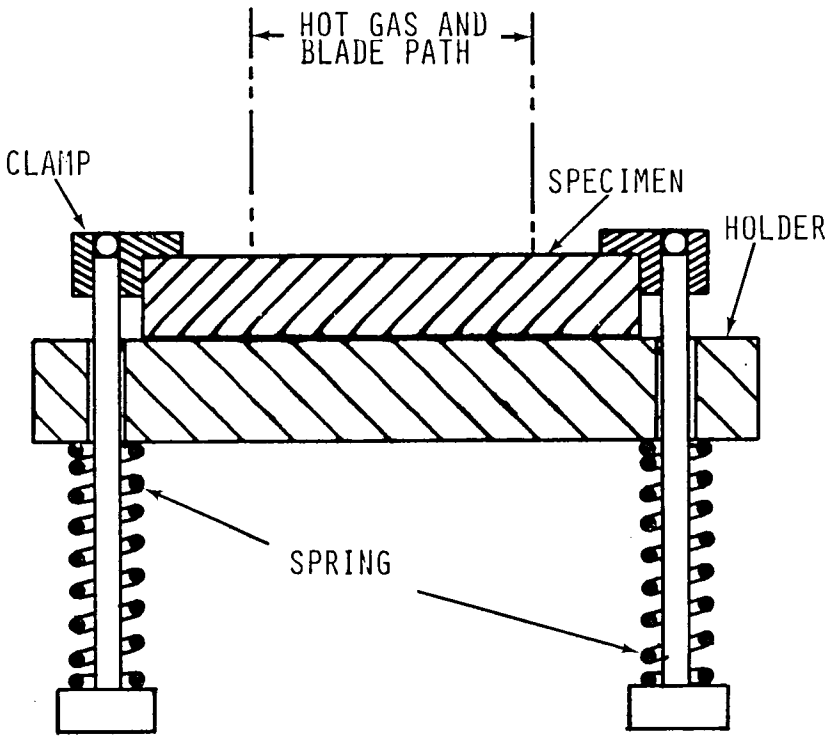

Figure 40. Specimen Retention at 1370°C

Table 5

Abradability at 1370°C

Silicon carbide 60% dense - 100/60 mesh	Sample demolished at initiation of contact.
Silicon nitride As-received 1/16 cell	Sample separated at nodal joints. Little blade wear. Abraded smoothly.
Silicon nitride As-received 1/32 cell	Specimen fractured during test. Indications of high blade wear prior to fracture.
Silicon nitride Filled 1/16 cell	Filler migrated to surface. Sample failed.
Silicon nitride Brazed 1/16 cell	High blade wear in node areas. Local braze failures and subsequent core loss.

3.5 BALLISTIC IMPACT TESTING

Ballistic impact testing for all samples was performed using the following test conditions:

Impingement angle	30 degrees
Velocity	127 mps
Projectile diameter	4.78 mm
Projectile weight	0.440 grams

After impact, samples were compared with respect to size of the impact damaged area, depth of projectile penetration, presence of surface cracking, and general loss of physical integrity (Table 6).

Representative specimens are shown in Figures 41 through 47. A silicon nitride specimen, 40 percent dense, is shown in Figure 41. One large fracture is evident originating at an impact crater. Significant penetration has occurred in both impact areas but overall damage is relatively light.

A similar silicon carbide specimen, Figure 42, exhibits appreciably more damage. Although the impact craters were approximately the same for both materials, severe delamination and cracking is evident in the silicon carbide material. The higher density abradables were less susceptible to projectile penetration. The 60 percent dense silicon nitride material, Figure 43, is free of craters and no major fracture was generated. Damage was limited to a slight loss of material (Fig. 44) in the immediate area of impact. The equivalent silicon carbide material was more susceptible to impact. The craters are deeper and some fracture occurred. The specimen shown was made from 60/100 mesh material. Specimens of the same density fabricated from -325 mesh fractured on impact.

Filled silicon nitride structures were also sensitive to impact. In Figure 45 the area of material loss is evident, large surface areas were lost with small local areas being totally expelled from the specimen. The cracks generated by impact were propagated through the structure in a manner similar to that observed in homogeneous ceramic materials.

Unfilled silicon nitride structures were relatively immune to crack propagation. Two are shown in Figures 46 and 47. In both cases, the projectile penetrated to form a typical impact crater. When sufficient energy had been absorbed the projectile rebounded leaving the structure undamaged except for the immediate area of impact.

Impact testing was not performed on the gradated silicon carbide specimens or the silicon carbide honeycomb. Both were experimental in nature and specimen quantity was limited. The abradability tests performed with these materials were considered to be of greater significance.

Table 6

Ballistic Impact Test Results at Ambient Temperature
(Velocity 127 mps, Impingement Angle 30 Degrees, 4.78 mm Steel Spheres)

			Damaged Area			
Test Series	System	Material	Length (mm)	Width (mm)	Depth (mm)	Comments
1	2	Corrugated Si_3N_4 2 mm cell size	30.5	8.9	6.4	Uniform crater ending abruptly as energy dissipated
2	3	Corrugated Si_3N 1 mm cell size	22.9	8.9	5.1	See above Test 1
3	10 & 13	Reaction bonded Si_3N_4 - 60° dense	*	*	*	No penetration, crack in sample at point of impact
4	12 & 15	Reaction bonded Si_3N_4 - 20% dense	11.4	4.4	2.5	Shallow crater with minor edge spalling
5	16	Silicon carbide 60% dense	**	**	**	Specimen shattered on impact
6	17	Silicon carbide 50% dense	6.4	3.2	1.3	Slight crack originating at impact area
7	18	Silicon carbide 40% dense	11.4	3.4	2.5	No crack formation. Penetration deeper than for silicon nitride
8	22 & 25	100/60 silicon carbide 60% dense	6.4	3.8	2.5	Deep short crater
9	23 & 26	100/60 silicon carbide 50% dense	16.5	6.4	5.1	Crater size approximately twice that of 60% dense material
10	24 & 27	100/60 silicon carbide 40% dense	**	**	**	Specimen delaminated upon impact
11	4	Filled corrugated silicon nitride 2 mm cell size	17.1	8.4	9.8	See test 1
12	5	Filled corrugated silicon nitride 1 mm cell size	10.5	7.2	5.1	See test 1
13	34	Reaction bonded silicon nitride 60% dense	*	*	*	No penetration, cracks in sample at points of impact
14	36	Sintered silicon nitride, 60% dense	**	**	**	Sample shattered. Cracks propagating from impact area

* Specimen showed no measurable loss.

** Specimen destroyed on impact.

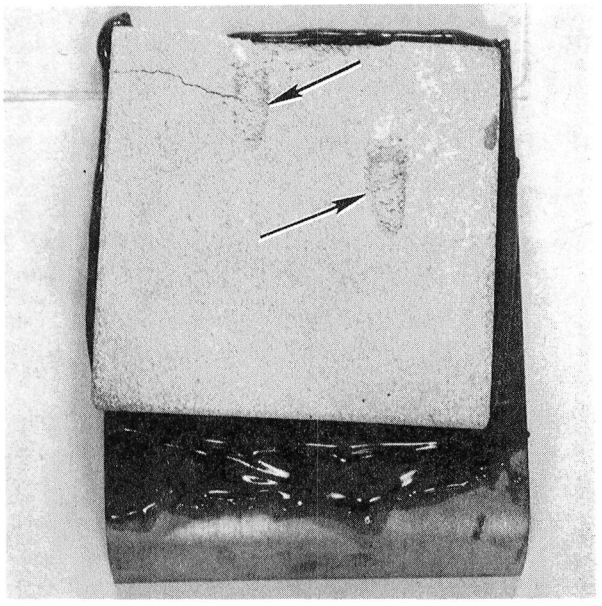

Figure 41.

Silicon Nitride 40 Percent Dense After Impact Test (Arrows Indicate Impact Area)

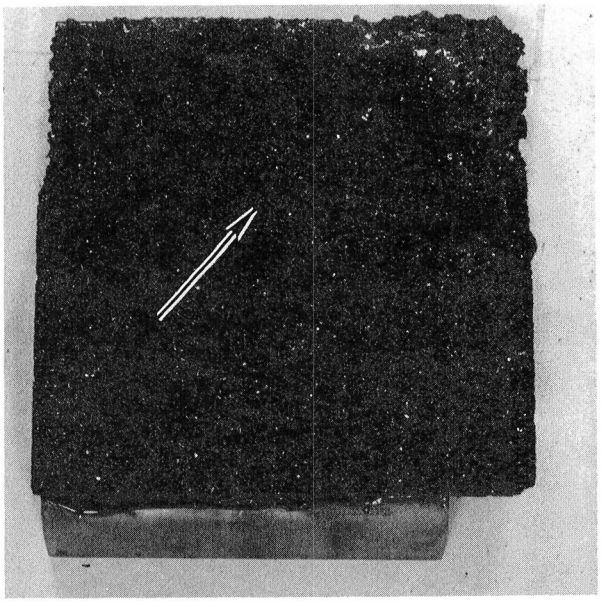

Figure 42.

Silicon Carbide 40 Percent Dense After Impact Test (Arrows Indicate Impact Damage)

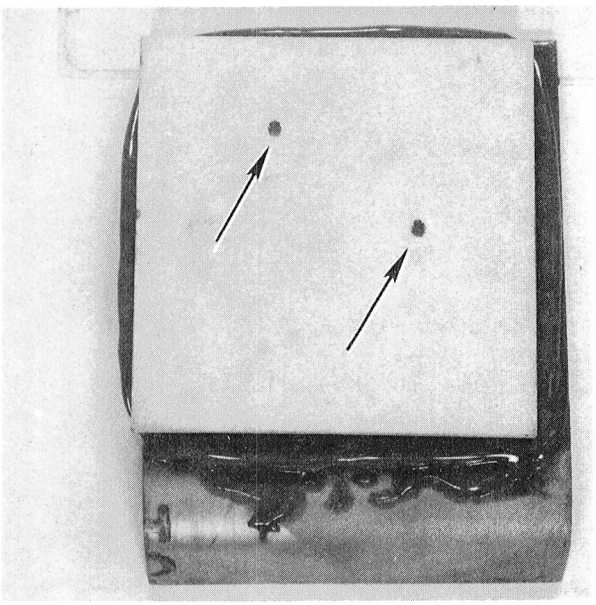

Figure 43.

Silicon Nitride 60 Percent Dense After Impact Test (Arrows Indicate Impact Area)

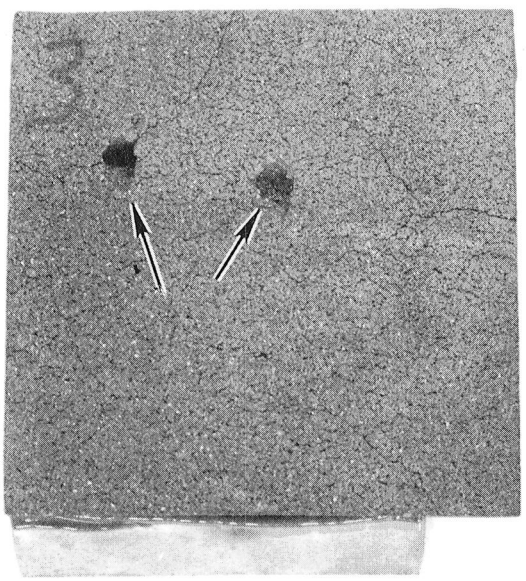

Figure 44.

Silicon Carbide 60 Percent Dense After Impact Tests (Arrows Indicate Impact Area)

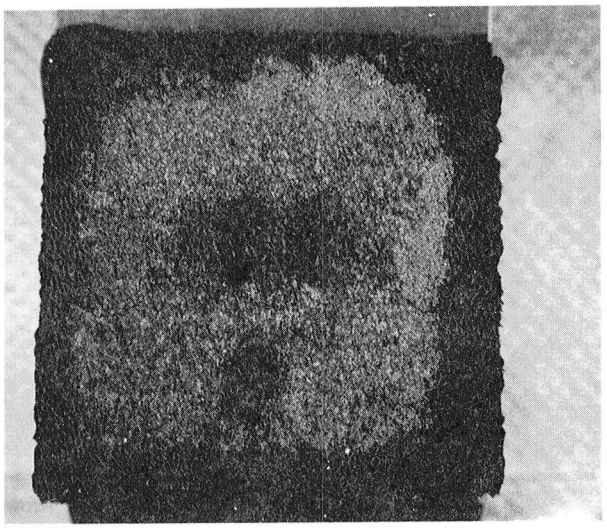

Figure 45.

Filled 1 mm Cell Silicon Nitride After Impact Test

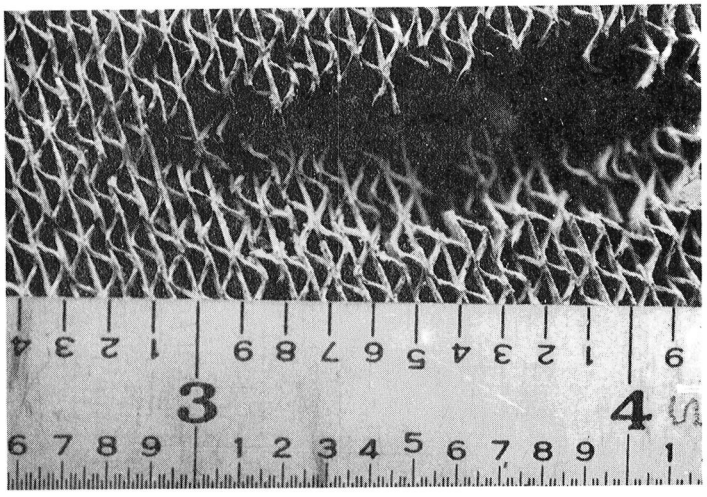

Figure 46.

Unfilled 2 mm Honeycomb Silicon Nitride After Impact Test

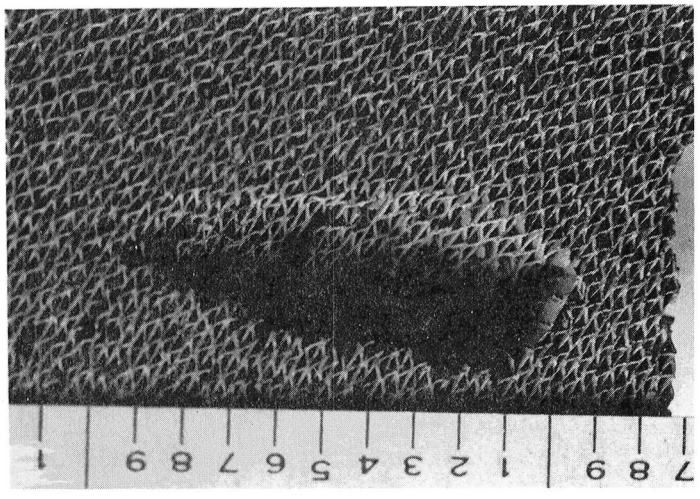

Figure 47.

Unfilled 1 mm Honeycomb Silicon Nitride After Impact Test

3.6 HOT GAS EROSION TESTING

Gas erosion tests were performed on filled and unfilled 1 mm cell silicon nitride and on reaction bonded silicon nitride (Figs. 48 through 52). Filler material was a mixture of silicon nitride powder and a silica glass. Test duration was 100 hours with a temperature of 1370°C at the sample surface. All samples were cooled to room temperature every 24 hours for inspection and weighing. The initial core structure, prior to filling or testing, was shown in Figure 5.

During the erosion test the filled structure suffered an almost complete loss of the filler material (Fig. 48). The glass component of the filler separated from the ceramic powder component at the high temperature and migrated to the honeycomb surface. The glassy component was then carried away by the high-velocity gases along with the silicon nitride filler. A parallel behavior was reported in static oxidation tests. In the latter, the glass (with ceramic particles intermixed) reached the surface where it remained as a glassy deposit in the absence of high-velocity gases. The glassy deposit was not analyzed chemically. Metallurgical examination indicated that the surface was primarily silica with some silicon nitride particles as inclusions.

Visual examination of the unfilled silicon nitride structure after 100 hours revealed the presence of a clear, glassy phase adhering to the cell inner walls (Fig. 49). This deposit resembles that observed in oxidation tests of the filled structure and the low-density materials based on silicon nitride. Metallographic examination indicated that a vitreous oxide was migrating to the surface during test.

Rounding and chipping of the ribbon edges also occurred during hot gas erosion testing of the honeycomb sample. Carbon deposits on the ribbon surfaces indicated high-velocity carbon particles were impacting on the exposed surfaces. This particle impact effect was also apparent on the low-density materials.

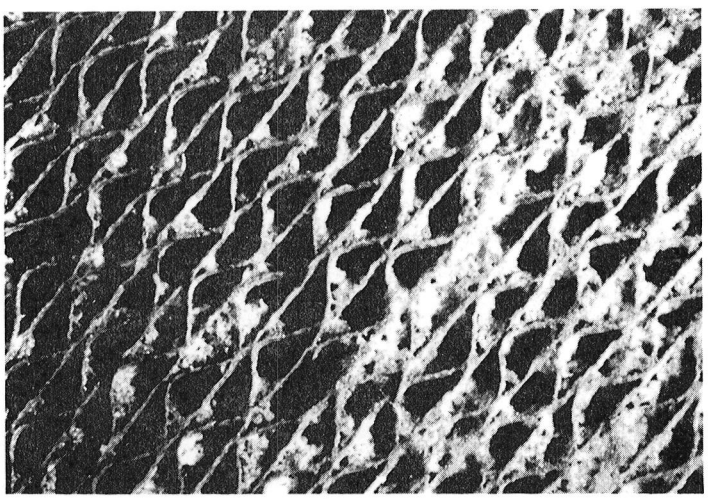

Figure 48.

1 mm Cell Unfilled Honeycomb Silicon Nitride Before Erosion Test

Magnification: 9.5X

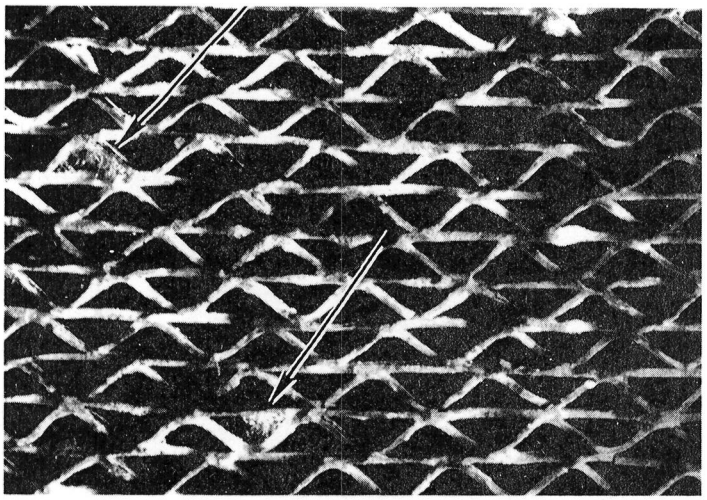

Figure 49.

1 mm Cell Filled Honeycomb Silicon Nitride After 100 Hours Hot Gas Erosion

Magnification: 9.5X

Arrows Point to Residual Filler

The surface of the reaction bonded silicon nitride material showed considerable pitting and coarsening after testing. A crater (Fig. 50) 0.91 mm in diameter can be identified as the origin of a hairline crack which extends through the full thickness of the sample. The effect was not localized as with the honeycomb silicon nitride structure. Figure 51 shows the continuation of the crack across the sample face. A glassy phase was also present on the surface of the reaction bonded sample. This phase is shown in Figure 52. Its formation tends to decrease surface roughness.

In the three material systems, weight gains were recorded rather than weight losses.

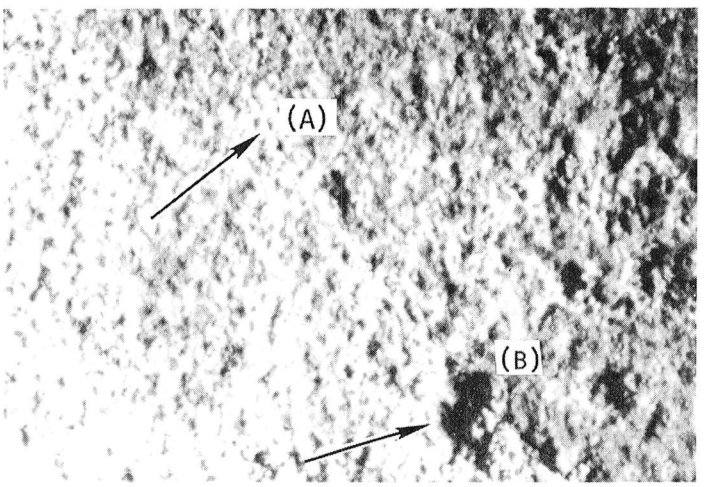

Figure 50.

Reaction Bonded Silicon Nitride After Hot Gas Erosion Test Showing Crack Propagation (A) From Impact Crater (B)

Magnification: 22X

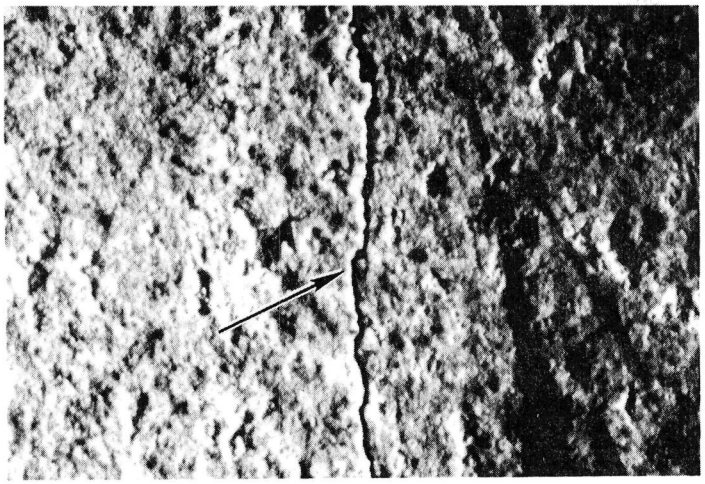

Figure 51.

Reaction Bonded Silicon Nitride After Hot Gas Erosion Test Showing Cracking Due to Particle Impact

Magnification: 22X

Figure 52.

Reaction Bonded Silicon Nitride After Hot Gas Erosion Showing Glassy Phase on Surface

Magnification: 22X

Additional hot gas erosion tests were conducted on silicon nitride honeycomb brazed to a high-density hot-pressed backing. Two specimens were tested initially. In both specimens, fracture and loss of honeycomb from the backing occurred. The fracture lines followed the braze fillet contour line. That is, failure occurred in the transition area between the braze fillet and free-standing honeycomb core ribbons.

Three thermocouples were located in the specimen to determine thermal gradients during test. Steady-state temperatures at the specimen front surface, bondline and the back surface were determined. The measurements were repeated 30 seconds after shutdown to determine temperature change rates and thermal gradients developed during test. Typical data is given in Table 7.

Table 7

Temperature of Backed Silicon Nitride Honeycomb
During Hot Gas Erosion Testing

	Steady-State Hot (°C)	After 30 Second Cool Down (°C)
Surface	1245	745
Bond line	948	745
Back face	701	634

Based on this data, cooling rates were:

Hot face	1000°C/min
Bond line	406°C/min
Backing	132°C/min

The hot face - bond line thermal gradient of 297°C during steady-state conditions was nearly twice the anticipatd 150°C predicted gradient. Thermal gradients and the resulting stress levels were thus well above anticipated values and none of the material systems were able to withstand these test conditions.

3.7 COMPRESSIVE STRENGTH

The variation in compressive strength with temperature for brazed silicon nitride honeycomb was determined. Test temperature was varied from ambient to 1370°C. The data obtained are summarized in Table 8 and Figure 53. The strength appeared to increase with temperature to a maximum at 1000°C. As the temperature was increased to 1370°C, no further increase was observed.

The response of the material system to compressive loading was characterized by initiation of failure at the contact surface. Fracture appeared to originate at point load areas. Once fracture was initiated, the load required to maintain compressive yielding of the material dropped to approximately 50 percent of the initial value, as shown in Figure 54. Fracture of the honeycomb was limited to the area subjected to compression loading. The failed area was uniform and free of preferred crack propagation through nodal or other areas.

Table 8

Compressive Strength of Silicon Nitride Honeycomb

Test Temperature	Failure Load (Newtons)	Failure Stress (MPa)	Mean Failure Stress (MPa)
Ambient			
No. 1	2000	218	
No. 2	1700	185	211
No. 3	2100	229	
No. 4	1950	213	
816°C			
No. 1	3100	339	
No. 2	3400	372	362
No. 3	3450	377	
1093°C			
No. 1	3800	415	
No. 2	4850	530	419
No. 3	3500	382	
No. 4	3200	350	
1260°C			
No. 1	3600	393	
No. 2	2800	306	355
No. 3	3350	366	
1427°C			
No. 1	4150	453	
No. 2	2650	407	407
No. 3	3300	361	

3.8 MODULUS OF RUPTURE

The specimens were coated with braze alloy prior to test to simulate their in-use condition. Backings were not used since their presence would mask the properties of the silicon nitride honeycomb material. Data is reported in Table 9.

The effect of temperature on the modulus of rupture (Fig. 55) was similar to its effect on compressive strength. Initially, the strength increased until a test temperature of 1000°C was achieved. Further temperature increases had only slight effect on the observed data.

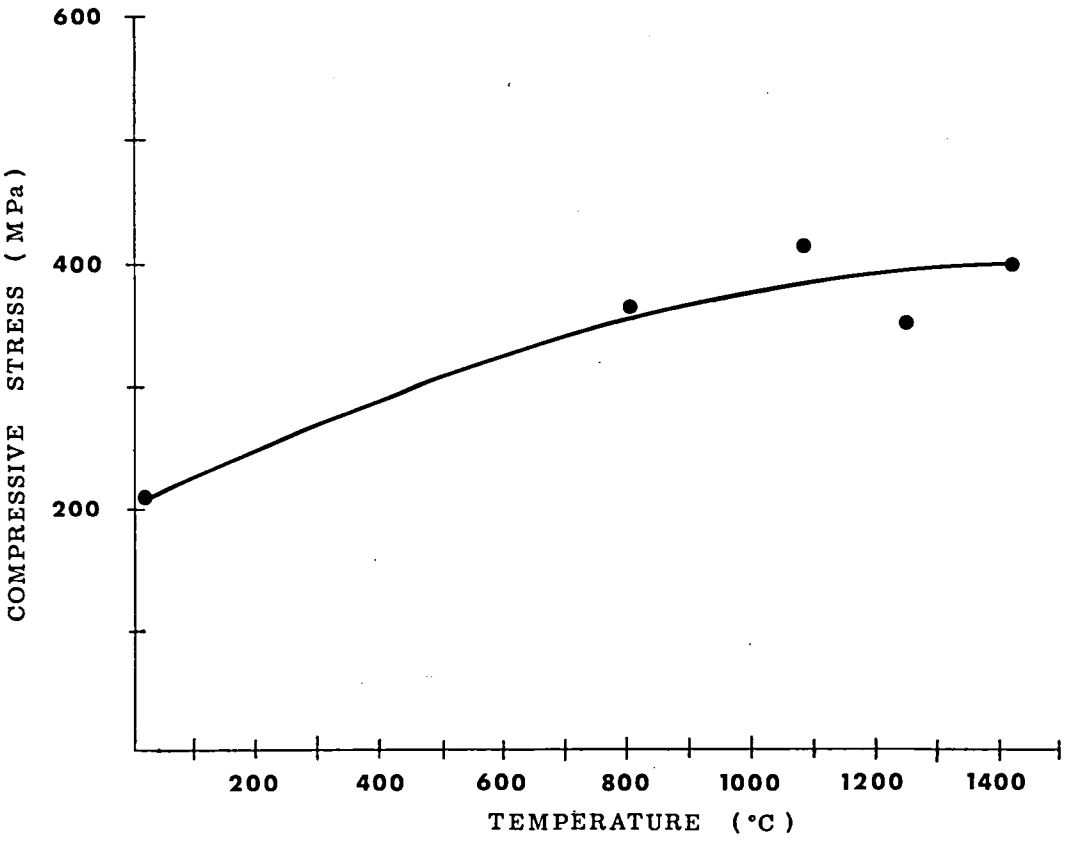

Figure 53. Compressive Strength of Silicon Nitride Ribbons in Silicon Nitride Honeycomb

At ambient temperatures fracture of the ceramic occurred, roughly parallel to the flat ribbon (i.e., breaks appeared in the sinusoidal ribbon, Fig. 56). As the temperature was raised, the preferred fracture direction became less distinct. Fracture occurred across both flat and sinusoidal ribbons (Fig. 57).

Generally, as the temperature was increased, the test data became more consistent with decreased variation between individual specimens.

3.9 PARAMETRIC ABRADABILITY TESTING

During baseline testing (Sec. 3.3) it was demonstrated that with conventional abradable materials, variations in rub conditions had a significant effect on performance. In those tests it was demonstrated that reducing ingression rate gave increased blade wear. The specimens were shown in Figures 37, 38 and 39. Similar tests to determine the effect of rub conditions were conducted with 1 mm cell honeycomb. These results are reported in Table 10.

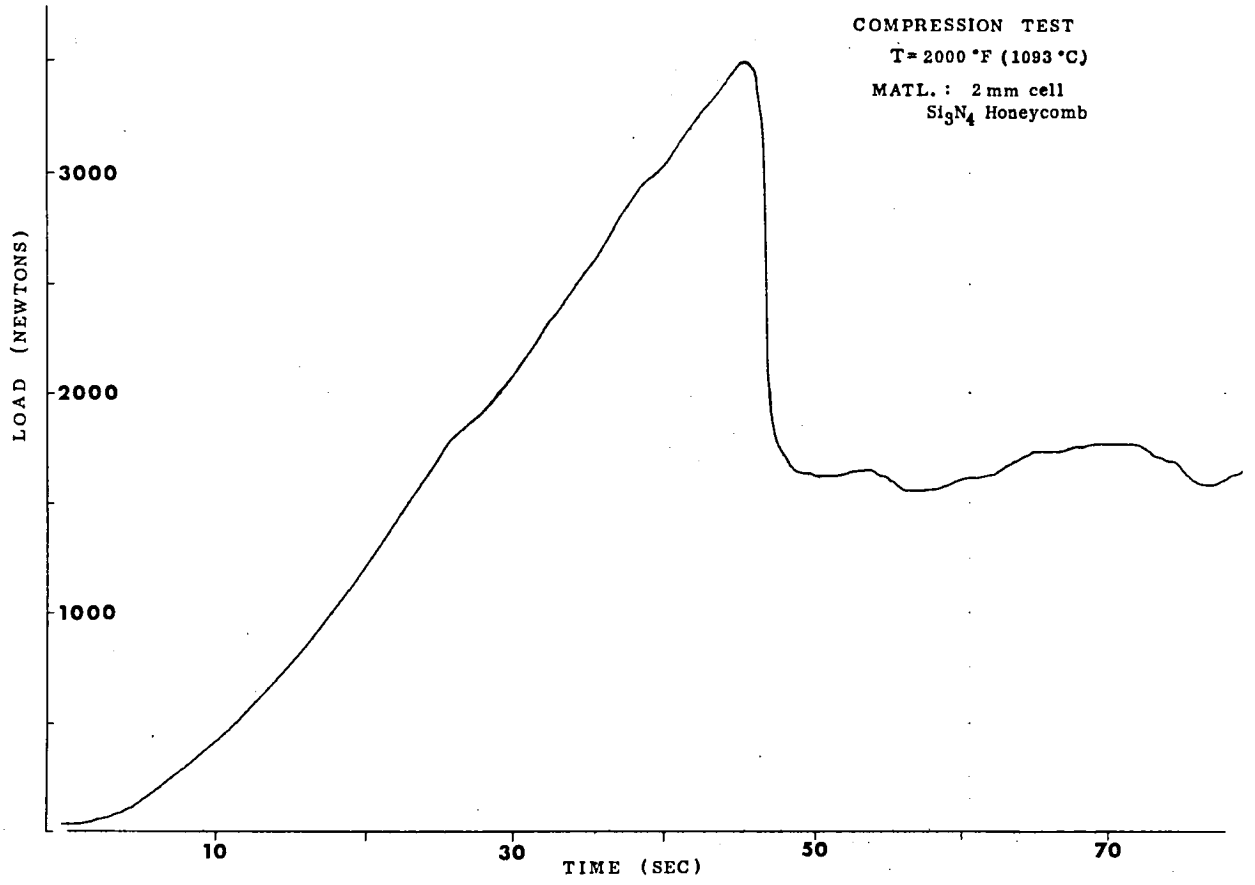

Figure 54. Typical Load Versus Time for Silicon Nitride Honeycomb

With the 1 mm cell structure a high ingression rate gave the best overall rub performance. The honeycomb structure was uniformly abraded with only slight scabbing. As the ingression rate and/or blade tip velocities were decreased abradable performance deteriorated. With the exception of the foregoing test and test No. 2, where partial fracture occurred, all of the remaining 1 mm cell silicon nitride abradable materials failed during test. Fragments recovered from these tests evidenced heavy scabbing. As the test temperature was increased failure became more rapid. The samples tested at 538, 982 and 1370°C failed upon contact with the blades and no significant data could be obtained regarding wear.

As can be seen in Table 10, only two runs indicated a trend toward improved performance with increased ingression rate. However, the consistent failure of the ceramic specimens limited the application of the data generated with the fine cell honeycomb.

Table 9

Results of Three-Point Bending Tests On 2 mm Cell Silicon Nitride Honeycomb

Test Temperature	Failure Load (Newtons)	Modulus of Rupture (MPa)	Mean (MPa)
Ambient			
No. 1	103	7.7	
No. 2	81	6.1	7.1
No. 3	101	7.5	
816°C			
No. 1	126	9.4	
No. 2	111	8.3	10.9
No. 3	201	15.0	
1093°C			
No. 1	376	28.0	
No. 2	191	14.2	21.1
No. 3	31	(1)	
1260°C			
No. 1	256	19.1	
No. 2	141	10.5	20.4
No. 3	426	31.7	
1427°C			
No. 1	296	22.1	
No. 2	300	22.4	21.9
No. 3	286	21.3	

(1) Sample failed in shear at the nodal bond.

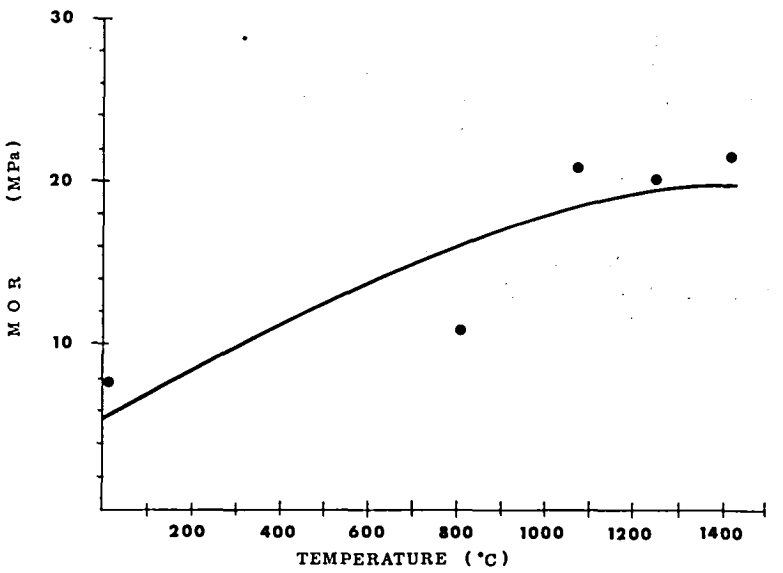

Figure 55.

Modulus of Rupture (MOR) of Silicon Nitride Honeycomb

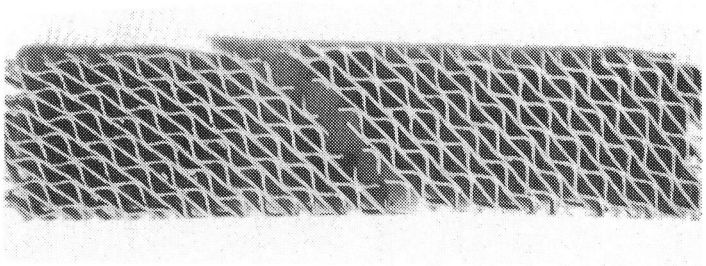

Figure 56.

Three-Point Bending Test at Ambient Temperature

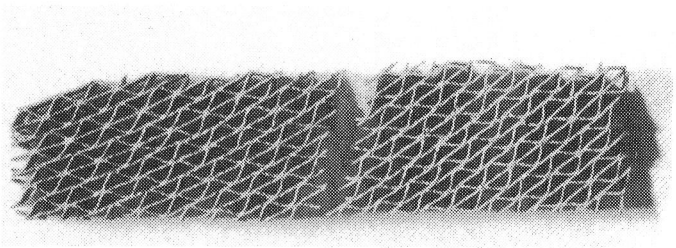

Figure 57.

Three-Point Bending Test at 1427°C

Table 10

Abradability of 1 mm Cell Silicon Nitride Honeycomb Under Varying Test Conditions

Test	Blade Tip Speed (mps)	Ingression Rate* (mm/sec)	Temperature (°C)	Abradable Wear (mm)
1	427	0.025	Ambient	1.090**
2	427	0.012	"	***
3	427	0.050	"	1.240
4	305	0.025	"	***
5	183	0.025	"	***
6	305	0.012	1370	***
7	305	0.012	982	***
8	305	0.012	538	***

* Rub depth 0.75 mm
** Partial sample fracture
*** Sample shattered during test

Tests conducted with 2 mm cell silicon nitride honeycomb exhibited less sample failure. Abradable wear was found to fall into two types of material removal:

1. Abrasive wear

2. Fracture near the surface.

The abrasive wear was characterized by a relatively uniform wear pattern of the test specimen with the depth being equivalent to the ingression. Fracture was evidenced by a loss of abradable well in excess of the interference. In the latter case, heavy scabbing, as shown in Figure 58, was frequently evident.

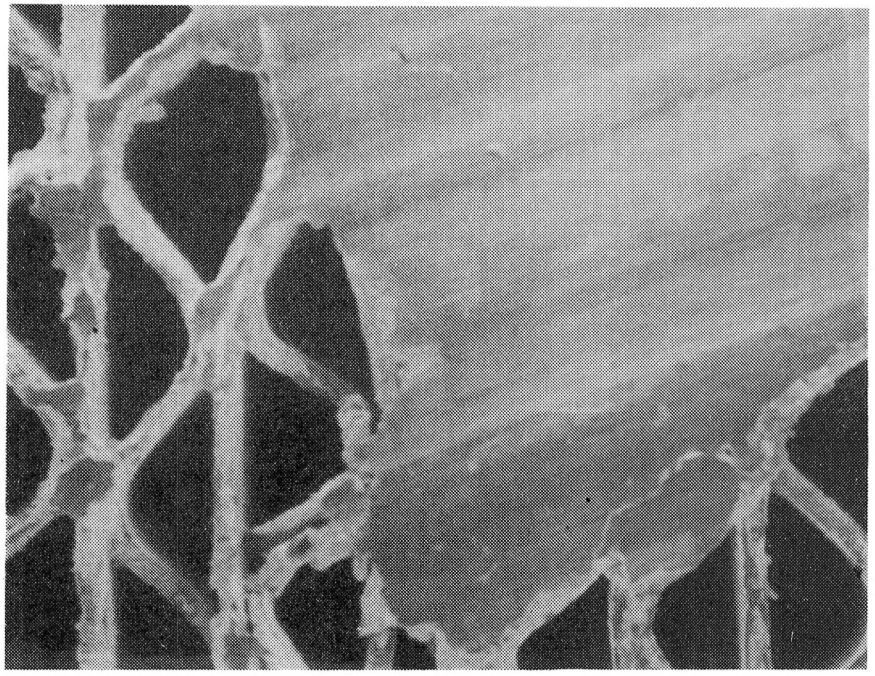

Mag: 10X

Figure 58. Blade Alloy Transfer to Silicon Nitride Honeycomb After Rub

The ambient temperature test results are summarized in Table 11. The baseline tests (1-6) have been grouped according to the type of wear observed. The first three are considered abrasive wear. The second three were fracture of the ceramic. No definitive pattern could be established regarding the effect of varying rub parameters on the ceramic honeycomb. The baseline specimens were equally divided between abrasive wear and fracture. Generally, the variations between the individual ceramic honeycomb specimens appeared to be greater than the variation in rub conditions. A trend was observed in that as the amount of material removed per blade impact increases (i.e., reduced tip speed or increased ingression rate) the tendency of the specimen to fracture increases. Both types of failure mode were observed at 427 mps blade tip speed at ingression rates of 0.025 mm/sec and lower. However, as tip speed decreased or ingression rate was increased, surface fracture of the specimen became a consistent result. Fracture depth was also consistent at 1.5 mm beneath the initial contact surface. Abrasive wear was also consistent in that the sum of the blade and shroud wear after test approximated 0.8 mm. Predicted wear total, without compensating for thermal growth due to rub, was 0.76 mm. Thus, the abrasive rub values were within normal experimental error.

Table 11

Ambient Temperature Abradability Tests
(2mm Silicon Nitride Honeycomb)

Test	Tip Speed (mps)	Incursion Rate (mm/sec)	Blade Wear (mm)	Ceramic Wear (mm)	Comments
1-3	427*	0.025	0.20	0.60	Abrasive wear
4-6	427*	0.025	0.15	1.5	Scabbing and fracture
7-8	427	0.012	0.08/ 0.20	0.86/ 1.5	Abrasive wear/ fracture
9-10	427**	0.05	0.12	1.5	Fracture
11	305	0.025	0.20	0.53	Abrasive wear
12	183	0.025	0.08	0.79	Abrasive wear and fracture
13	91	0.025	0.10	1.5	Fracture

* Average values from three tests
** Average values from two tests

The effect of temperature on rub performance was more consistent, as shown in Table 12. Blade wear varied inversely with temperature. At 1370°C blade wear was barely detectable. As the temperature decreased, blade wear became greater although no significant decrease in abradable wear was observed. The ceramic specimens were also relatively free of the scabbing that occurred in the ambient temperature test.

Table 12

Abradability Tests at Selected Temperatures
Using 2 mm Silicon Nitride Honeycomb

Temperature (°C)	Blade Wear (mm)	Ceramic Wear (mm)	Comments
1370	0.03	0.76	Abrasive
982	0.15	0.74	Abrasive
538	0.20	0.76	Abrasive

Tip speed - 305 mps
Ingression rate - 0.012 mm/sec
Ingression depth - 0.76 mm

In addition to the specific results cited, several visual observations were made during these tests.

1. Scabbing was greatest at the airfoil trailing edge.

2. Scabbing decreased with increasing test temperature.

3. Test results were more consistent at elevated temperatures and less susceptible to failure through material variations.

3.10 JOINING OF SILICON NITRIDE ABRADABLES TO HIGH-DENSITY BACKINGS

Initially, readily available high-temperature glasses, as listed below, were tested by furnace exposure at 1232°C for long-term stability.

- 50 percent GN19* - 50 percent fused silica
- Carborundum cement
- Aremco** (zirconia base)
- Ultrabond** (alumina base)
- Ceramabond** (alumina base)

* A high-temperature Solar developed glass
** Aremco Products, Inc.

Their suitability for this application was judged on the basis of the following criteria:

- Chemical, thermal and mechanical stability to 1232°C for extended time periods when heated in air.
- Dimensional stability through repeated thermal cycles.
- Ability to wet silicon nitride materials without excessive attack.
- Suitability for application and processing using conventional techniques.

All of the cements exhibited poor wetting characteristics and a subsequent loss of adherence when used on hot-pressed silicon nitride. After test the joint was weak and unsuitable for end use application. The glasses provided adequate wetting and good adherence. However, after furnace exposure in air at 1093°C for 500 hours, the interface was destroyed by reactions between the silicon nitride and the glass bonding agent. A typical specimen is shown in Figure 59. The glass reacted with the silicon nitride to form a brittle crystalline phase in the glass and silica-rich zones in the silicon nitride. The resultant structure is brittle and subject to failure during normal thermal cycling.

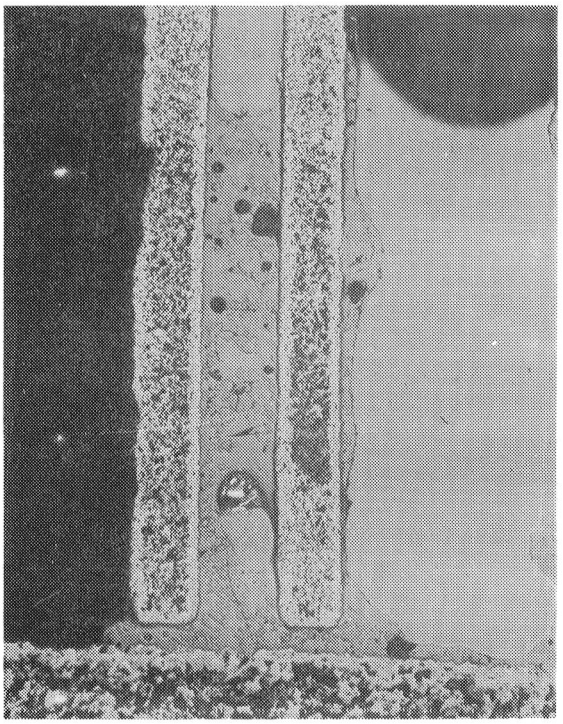

Figure 59.

Silicon Nitride Bond Using Silica-GN19 High-Temperature Glass Bond

Magnification: 40X

Silicon alloys were selected as a possible alternate to the cements and glasses. Silicon powder with zero to ten percent titanium additions was evaluated. Wetting tests were conducted in argon and in vacuum. The titanium addition was made to enhance wetting.

The specimens fired in an argon atmosphere exhibited poor wetting characteristics. Figure 60 illustrates the lack of wetting in argon achieved using a two percent titanium addition. Similar tests using one and ten percent additions with hot-pressed silicon nitride are shown in Figure 61. No benefit was gained from the change in titanium content. The specimen containing ten percent titanium exhibited a visible oxide film on the surface.

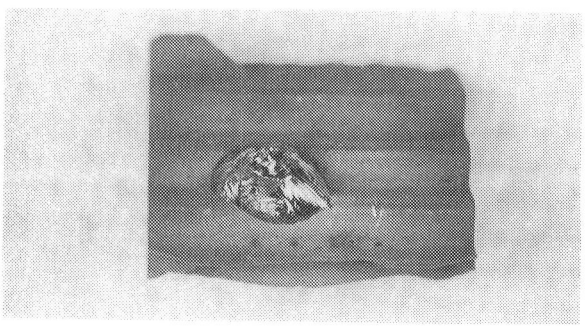

Figure 60.

Lack of Wetting of Reaction Bonded Silicon Nitride by Silicon-Two Percent Titanium Fired in Argon at 1482°C

Magnification: 4X

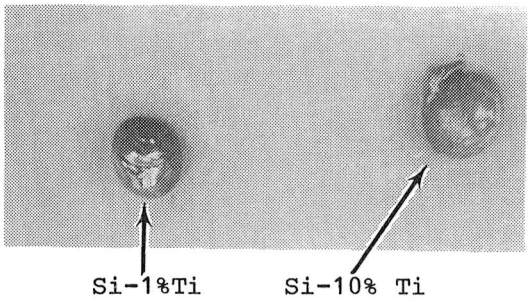

Figure 61.

Effect of Titanium Additions to Silicon on Wetting of Silicon Nitride at 1538°C in an Argon Atmosphere

Magnification: 2X

Wetting tests were then conducted in a vacuum using the same materials. The wetting of hot-pressed silicon nitride by silicon-one percent titanium is shown in Figure 62. Wetting characteristics are excellent. Further additions of titanium did not improve the wetting. At ten percent titanium addition, an oxide film formed that reduced flow, as shown in Figure 63 . Similar results, Figure 64, were obtained with reaction bonded silicon nitride. The alloy wetted uniformly with good flow characteristics. In subsequent tests, similar results were obtained without the titanium addition and its use was made optional. These tests were used as a basis for subsequent joining of silicon nitride specimens used in this program. An initial braze joint is shown in Figure 65. Reduced joint gap and increased braze alloy was used to produce subsequent bonds. A typical honeycomb braze joint is shown in Figure 66. Wetting and flow is similar to that achieved in conventional braze joining of metal honeycomb. The alloy provided small fillets and traversed nodal joints in the conventional manner.

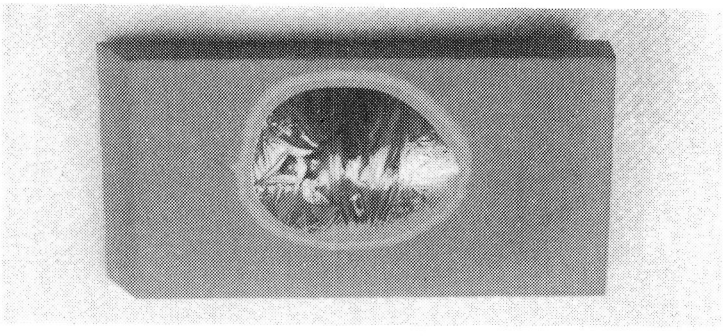

Figure 62.

Wetting of Hot-Pressed Silicon Nitride by Silicon-One Percent Titanium When Fired in a Vacuum at 1482°C

Magnification: 2X

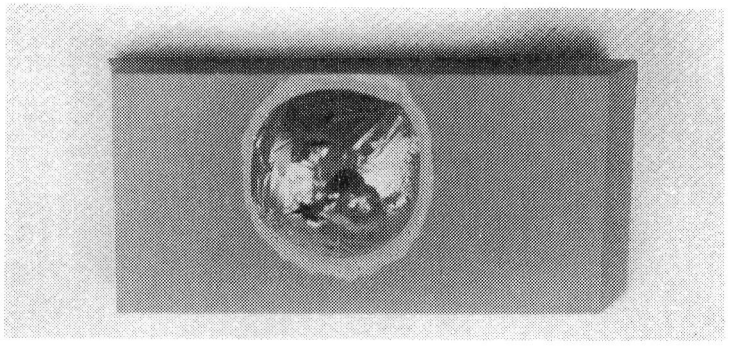

Figure 63.

Wetting of Hot-Pressed Silicon Nitride by Silicon-Ten Percent Titanium in Vacuum at 1482°C

Magnification: 2X

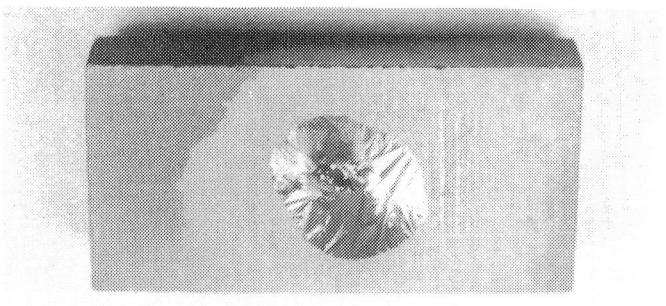

Figure 64.

Wetting of Reaction Bonded Silicon Nitride by Silicon-Ten Percent Titanium at 1482°C

Magnification: 2X

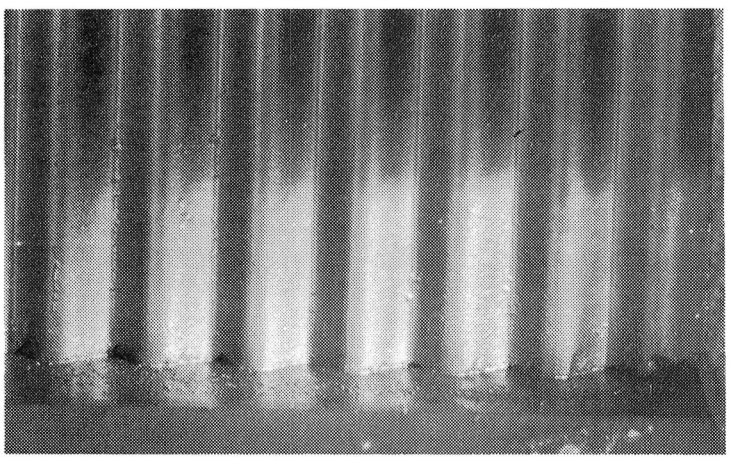

Figure 65.

Braze Joint of Silicon Nitride Honeycomb to a Hot-Pressed Backing With Minimal Filler

Magnification: 4X

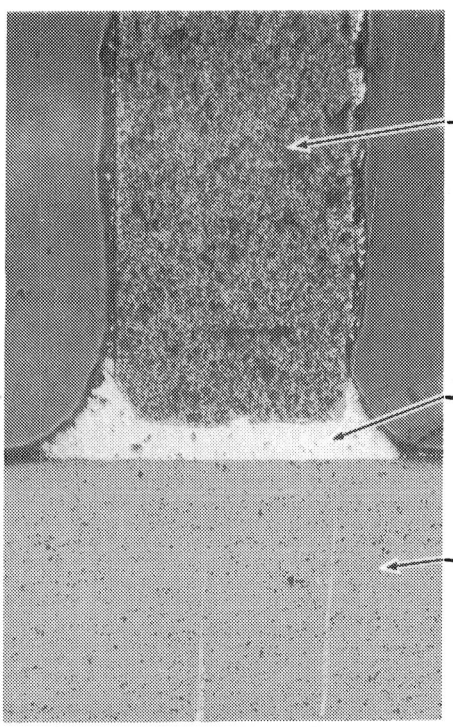

Magnification: 75X

Figure 66. As-Brazed Bond Between Silicon Nitride Abradable and Hot-Pressed Silicon Nitride Backing

After joining silicon nitride honeycomb specimens by brazing, specimens were tested for thermal stability by furnace exposure in air at 1232°C for 500 hours. A typical section is shown in Figure 67. No significant deterioration of the joint developed. Further testing at 1371°C, Figure 68, indicated that the upper temperature limit for this system lay between the two temperatures. Significant interaction developed between the braze alloy and the ceramic at 1371°C, creating cracks in the ceramic phase and degradation of the system.

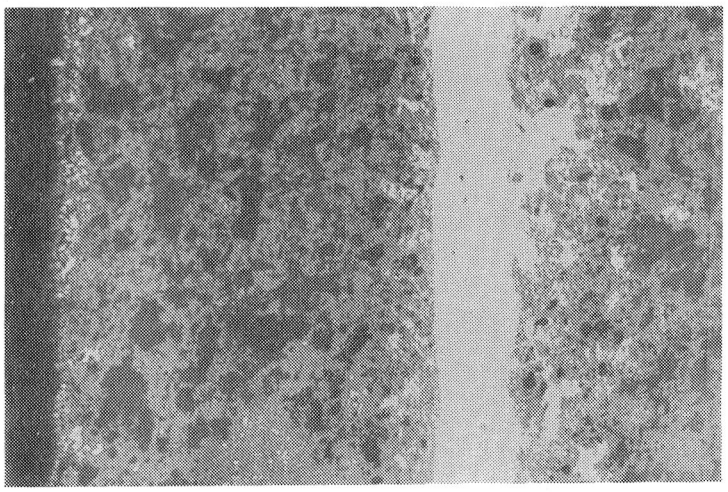

Figure 67.

Brazed Silicon Nitride Interface After Thermal Stability Test at 1232°C

Magnification: 250X

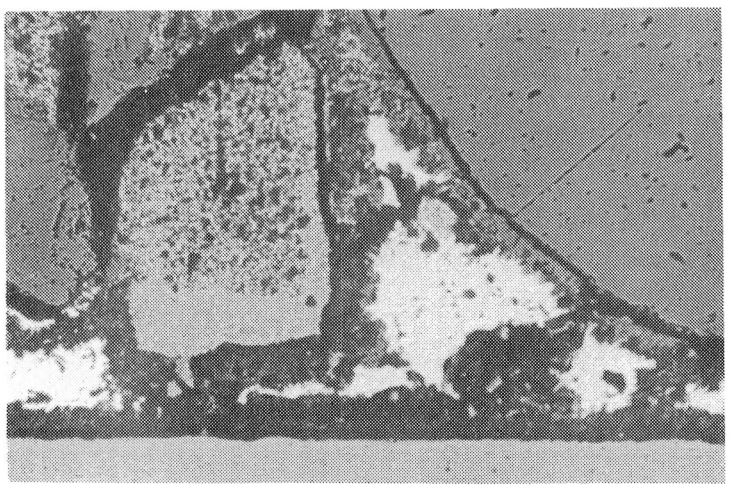

Figure 68.

Silicon-Silicon Nitride Braze Joint After 500 Hours at 1371°C

Magnification: 75X

3.11 CERAMIC BLADE TIP ANALYSIS

The need for increased blade tip wear resistance through use of ceramic inserts required that a design analysis be performed. This task was divided into two phases:

Phase I - Insert Geometry

Phase II - Application to an Available Engine

The results of each are briefly reported in the following sections.

3.11.1 Insert Geometry

For selection of tip geometry a mechanical stress analysis was performed for spin and rub stresses. The latter analysis was limited by the availability of data on frictional and similar properties of the selected material system, hot-pressed silicon nitride tips and silicon nitride honeycomb.

Four configurations of blade tip insert were selected for initial analyses. These are sketched as Figures 69, 70, 71 and 72 under maximum compressive rub loading conditions. The "T" insert (Fig. 72) was dropped at this point. Lateral support against shear forces generated during rub was limited and high localized stresses from minor deviations in tolerances would create excessive stress levels.

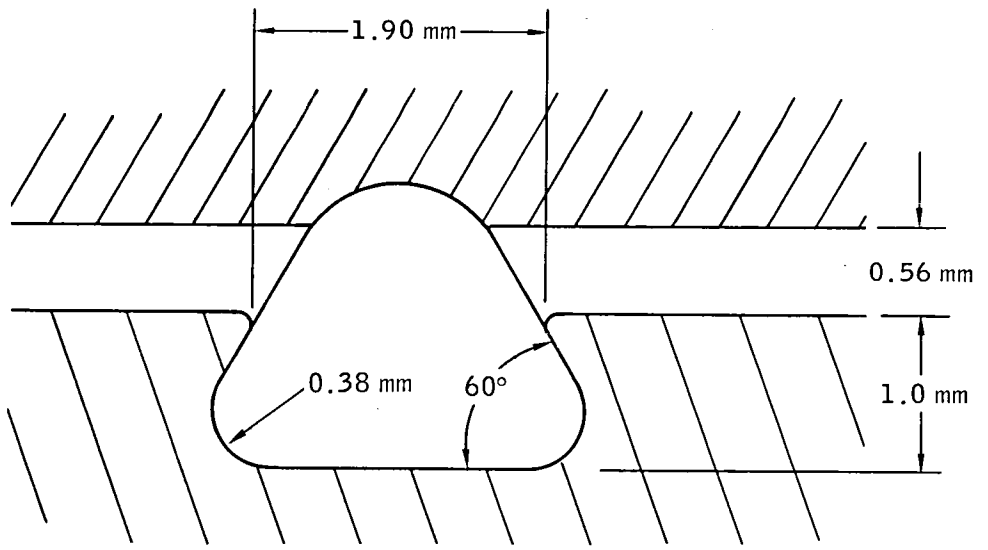

Figure 69. Triangular Insert With Minimum Clearance

The minimum clearance triangle insert was analyzed for thermal stresses anticipated during rub. Initial calculations predicted that comprehensive stresses in excess of 175 MPa would be developed. These stresses resulted from the lack of provision for differential thermal expansion between the blade and insert. Stress would become especially severe when rub occurred with high energy inputs to the blade tip. The energy input rates would exceed the ability of the tip to transfer heat to the metal blade. In addition, machining and assembly tolerances for this concept were impractical. Closely

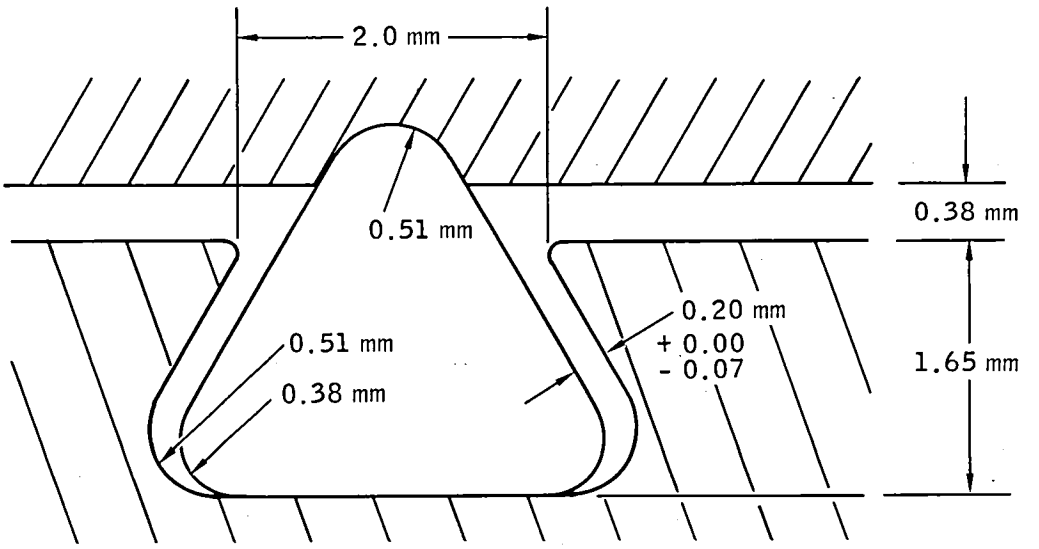

Figure 70. Triangular Insert With 0.20 mm Clearance

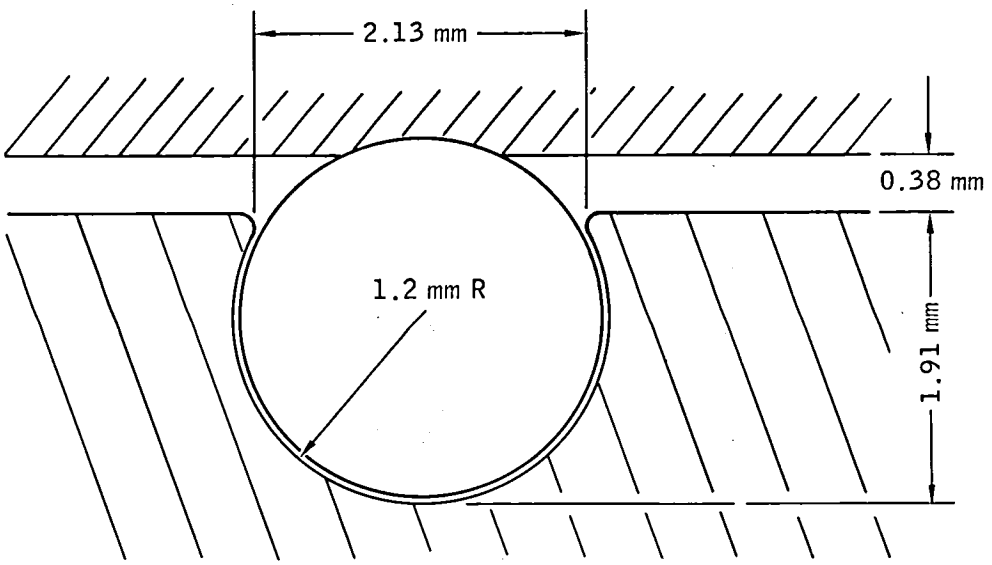

Figure 71. Cylindrical Insert With 0.025 mm Clearance

controlled dimensions would be required to obtain firm insert retention. Except by selective fit and hand polishing, the presence of high localized stresses due to surface irregularities could not be avoided.

The cylindrical concept (Fig. 71) was attractive from a manufacturing and assembly viewpoint. Tolerance could be easily achieved with conventional methods at a relatively low cost. However, further study indicated rub would limit its effectiveness. During rub one of two conditions would develop:

1. the cyclinder would rotate

2. the cylinder would remain stationary.

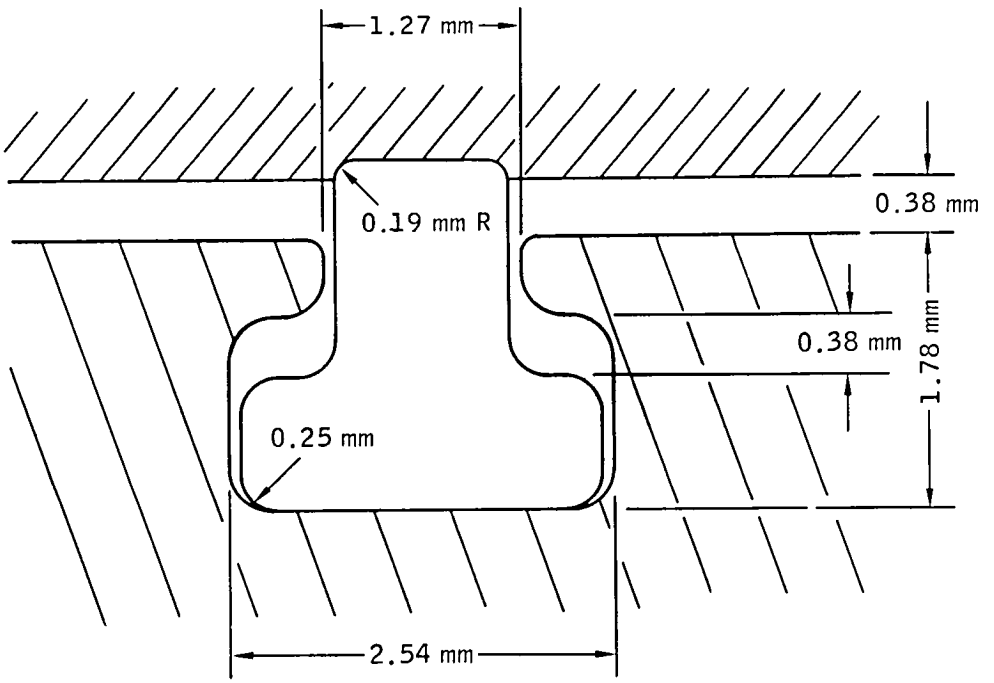

Figure 72. "T" Insert With 0.38 mm Clearance

In the first case, extremely high frictional heating was anticipated between the insert and the blade tip insert contact surface, leading to galling and material transfer. These would then lead to pressure points and insert failure. In the second case, local tip flattening was considered probable during initial rub. Subsequent partial rotation would result in the localized stress concentrations shown in Figure 73. Various anti-rotation concepts were considered but no practical solution was found. These concepts included grooves in the insert, notches in the insert end, flats on the insert base, etc., all of which would correspond with matching configurations in the blade tip. As in the previous case, to be effective, extremely close fits are required introducing manufacturing problems and the probability of excessive localized stress.

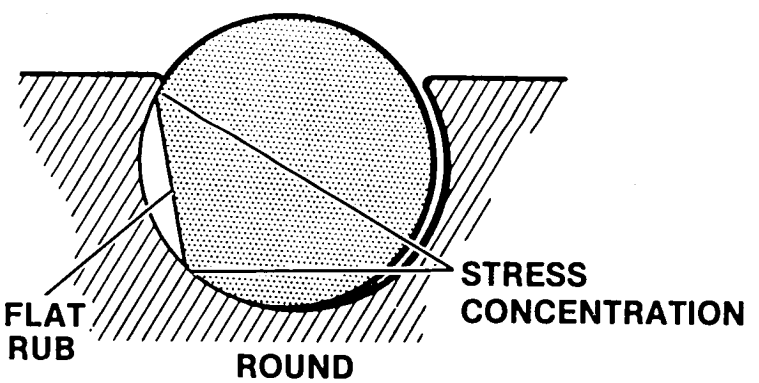

Figure 73.

Circular Insert After Initial Rub

The triangular tip with increased assembly and operating clearances (Fig. 70) was then analyzed for further study. Thermal and vibrational analysis established that no major problems existed with this configuration, providing proper assembly clearances were maintained. It was therefore selected for further study as an operating turbine blade.

3.11.2 Application to an Available Engine

A second-stage turbine blade from a Solar production engine was selected for this portion of the analysis. Operating conditions for this engine are as follows:

Tip speed	418 m/sec
Rub depth, maximum	0.76 mm
Rub depth, normal	0.25 mm
Seal temperature	760°C (minimum)
Blade alloy	MAR-M421

The temperature is considerbly below that of the proposed ceramic seal. However, at present, documented baseline data for design analysis and test evaluation is not available for a 1370°C seal in a working engine. The selected blade is in current use and its rub characteristics are well documented from normal service. This data can be used as a baseline in evaluating the performance of the ceramic tip insert.

Analytical studies of this type are limited by the amount of available data. To fully predict tip performance, experimental data must be generated. Carruthers, Walker and Van Wanderham (Ref. 1) demonstrated some of the difficulties encountered in analytically predicting behavior for a metal-ceramic hybrid system. In their work, a ceramic bladed rotor was developed. This unit combined a metal disc with ceramic blades retained by a dovetail attachment. A careful design analysis was performed based on all available data. However, premature failure occurred during test. Failure analysis after test showed that cyclic fatigue due to normal equipment speed variations of one to two percent and a thermal gradient of 94°C materially contributed to this failure. They concluded that the initial analysis must be followed by a test program to correlate the experimental data with that used in the analysis. The differences obtained between the experimental and predicted performance would then be used to refine the analytical study.

The silicon nitride design properties used in the analysis were derived from Uy, Williams and Swank (Ref. 2). As part of their study of the potential for ceramic components in gas turbine engines, they have experimentally determined physical properties for several grades of silicon nitride. In Reference 3 tables of design properties are given for silicon nitride. These were used in the design calculations.

The tip geometry selected for initial test is shown in Figure 74. The tip is designed for insertion into eloxed slots originating at approximately 33 percent of the airfoil contour. After insertion a contoured retainer will be

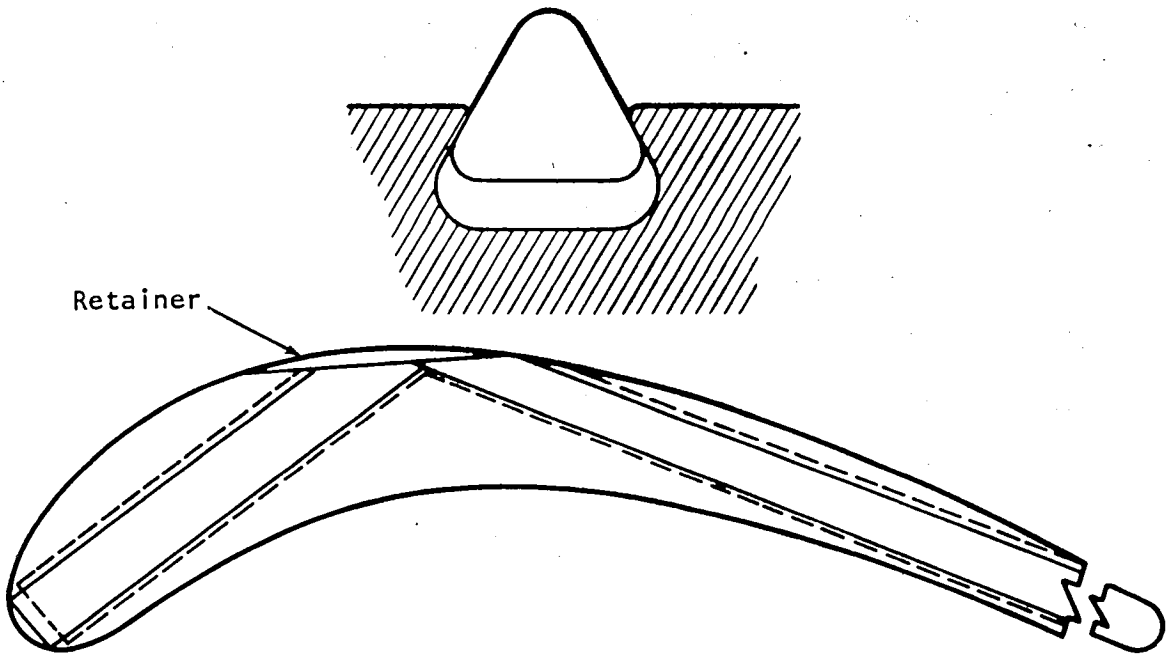

Figure 74. Ceramic Blade Tip Insert

attached to prevent tip losses and deviations on the airfoil surface. Design characteristics of the insert are given below.

Blade material	MAR-M421
Tip material	Hot-pressed silicon nitride
Base width	2.03 mm
Height	2.41 mm
Edge radius of slot	0.51 mm
Edge radius of insert	0.38 mm
Tip to slot clearance	0.38 mm
Slot depth	1.65 mm
Design rub depth	0.76 mm maximum 0.25 mm design

As stated previously, the analytical study was limited by availability of data. The brief duration of rub during engine operation makes dynamic factors such as vibration small. Once clearance between the insert and tip shoe

have been established, steady-state conditions exist and vibrational effects are limited to low-frequency, high-amplitude modes. The damping effect of the insert on the blade could not be predicted from available data. This characteristic can only be determined by laboratory test. The current results from tip stress analysis are tabulated and reported below for normal engine operation at 11,168 rpm with a tip speed of 427 mps.

Centrifugal tip load	0.41 MPa
Pressure face loading	0.8 MPa
Tip shear stress	2.0 MPa
Bending stress	3.6 MPa
Maximum tip stress	27.3 MPa

These initial results from the design analysis show that stresses are well within the limitations of silicon nitride at 760°C.

4

NEW TECHNOLOGY BRAZING OF SILICON NITRIDE

During the program a reliable technique was developed for joining silicon nitride by brazing techniques using silicon with and without titanium additions. The procedure is given in detail in this section for application to other areas. Titanium content may require adjustment to adapt to specific silicon nitride compositions. The procedure described has been found to work well with materials used in this program. The braze alloy can have zero to [illegible] percent titanium additions with joint gaps of less than 0.13 mm.

4.1 BRAZE ALLOY

Composition

Titanium (adjust to control flow)	- 0-10%
Impurities	- 1% maximum
Silicon	- Balance

Particle Size Distribution

Sieve Number U.S. Standard	Sieve Opening (μm)	Percent Through
170	88	100
270	53	70-80
325	44	55-65

4.2 BASE MATERIALS

Hot-pressed silicon nitride	>99% dense
Reaction-bonded silicon nitride	>75% dense

4.3 PREPARATION

4.3.1 Fit components as required to provide a 0.025 to 0.076 mm gap.

4.3.2 Solvent clean with methyl ethyl ketone or other solvent to remove residue and other surface contaminants.

4.3.3 Apply thin coating of Nicrobraze cement (Wall Colmonoy, Inc., Detroit, Michigan) to each surface to be joined.

4.3.4 Deposit excess braze alloy powder to coated surface and remove excess braze alloy.

4.3.5 Assemble and fixture to maintain relative component location.

4.4 BRAZING

4.4.1 Place assembly in a vacuum furnace and reduce pressure to a maximum of 10^{-5} mm Hg.

4.4.2 Heat assembly to 150°C $\pm$5°C and hold until pressure stabilizes, indicating completion of outgassing.

4.4.3 Increase temperature to 1482°C $\pm$20°C and hold for five minutes.

4.4.4 Furnace cool to 150°C or lower and remove parts from furnace.

4.5 INSPECTION

4.5.1 Examine joints for uniform fillet and braze flow. Large voids are indicative of excessively rapid heating to 150°C or insufficient dwell time to complete outgassing. Poor wetting, as indicated by limited braze flow, indicates contamination of the materials or atmosphere.

5

CONCLUSIONS

Testing of abradable ceramic materials for use in turbine tip seals at 1370°C has shown that ceramics have good potential. Silicon nitride honeycomb type structures possessed good abradability and were resistant to oxidation and impact damage.

Low-density structures fabricated from silicon carbide of relatively coarse, 60 and 150 mesh grain size had excellent abradability but limited erosion resistance. They were also difficult to attach to a high-strength backing for mating with a metal substructure.

The test evaluation of ceramic tip inserts demonstrated that hot-pressed silicon nitride was superior to silicon carbide and resistant to fracture during rub. An analytical study of the tip inserts confirmed these results. Design analysis based on a current production engine blade led to the conclusion that a tip insert with a triangular cross-section would withstand the stresses developed in engine operation. Rub testing of the silicon nitride tip inserts showed their wear to be one-fifth to one-tenth that of an equivalent superalloy tip.

Investigation into the effect of changes in rub conditions on the performance of abradable blade tip seals showed that increased temperature improved abradability. It also indicated that for a given combination of materials and depth of rub, increasing the penetration rate reduced tip wear. In general, as the amount of material removed per blade impact increased the relative blade wear decreased. Light rubs tended to initiate scabbing of the abradable, leading to high blade wear in subsequent rubs.

Joining of silicon nitride abradables to high-density backings of the same material can be accomplished by brazing in a vacuum with silicon containing minor additions of titanium. Close control of joint gap and braze alloy placement is required to produce reliable joints.

During the test program numerous failures were encountered during test due to thermal stresses. Also, variations between individual specimens sometimes produced conflicting test results. These problems were largely due to use of materials initially produced for less severe applications. In future test programs these difficulties can be largely eliminated. This requires concentrating on the two most successful abradables (i.e., silicon nitride honeycomb and 60 percent dense silicon carbide) and optimizing the structures and processing controls.

6

RECOMMENDATIONS

From this work a candidate high-temperature abradable tip seal material emerged - reaction bonded silicon nitride in a honeycomb structure. The material has the potential for use at 1370°C. Additional structural analysis, fabrication development, and testing to optimize cell size, wall thickness and cell depth is required.

The program also demonstrated the effectiveness of silicon and silicon-titanium as braze alloys for joining hot pressed silicon nitride to reaction bonded silicon nitride. The brazement is oxidation resistant to above 1200°C. Other, slightly modified, alloys may need to be investigated that will provide for wider gap brazing and improved strength and oxidation resistance to 1370°C in future applications.

The design analysis tests of hot-pressed silicon nitride blade tips indicate triangular tip inserts should be carried forward to final design and engine test.

Ceramic tip seal systems of the types investigated show great promise in providing good thermal stability, abradability, and corrosion resistance to 1370°C. Their development should receive a high priority in our energy conservation efforts to increase gas turbine performance and efficiency.

APPENDIX A

ABRADABILITY TESTING RIG

APPENDIX A

ABRADABILITY TESTING RIG

Abradability tests were performed using the Solar seal test facility. The test rig, illustrated in Figure 75, is powered by an air driven turbine adapted for this application from one of Solar's standard production engines. Air to drive the turbine is supplied at a pressure of 260 MPa with a mass flow of 1.4 Kgs/sec. The turbine is directly coupled to the output shaft through a flexible coupling. Abradable tip seal materials are tested at speeds of up to 427 mps and test temperatures to 1370°C. Figure 76 shows a 356 mm diameter A-286 alloy turbine disc broached with six MAR-M421 alloy turbine blades. The blades have been eloxed on the tips to simulate squealer tips. The disc and blade temperatures are limited to 650°C by air cooling during elevated-temperature testing.

The seal material under evaluation is located immediately below this disc on a platform advanced by a variable speed motor. The platform and seal material are instrumented with strain gages and thermocouples to obtain force and temperature data for each test.

The rig setup in Figure 77 is used for elevated-temperature tests. One broached blade slot was unused in this case due to the nature of the test. For high-temperature tests (a honeycomb tip seal is shown), the setup includes the addition of oxygen-MAPP gas torches to heat the seal material to the test temperature and shielding to reduce heatup of the wheel and bearing housing. The test parallels the air-cooled blades with respect to an uncooled seal.

A sample configuration is shown in Figure 78. This sample is radiused to match the blade tip diameter. The configuration was selected to allow evaluation of a large number of materials at a reasonable cost.

As noted in the text, abradable temperatures of 1370°C were achieved with this test setup. Consideration has been given to additional disc cooling to allow higher blade temperatures. However, this has not been installed at present.

In Figure 79 typical reworked turbine blades used in this test facility are shown. These are made from standard engine blades by trimming off the excess blade length, mounting the stubs in a disc and grinding to the final diameter.

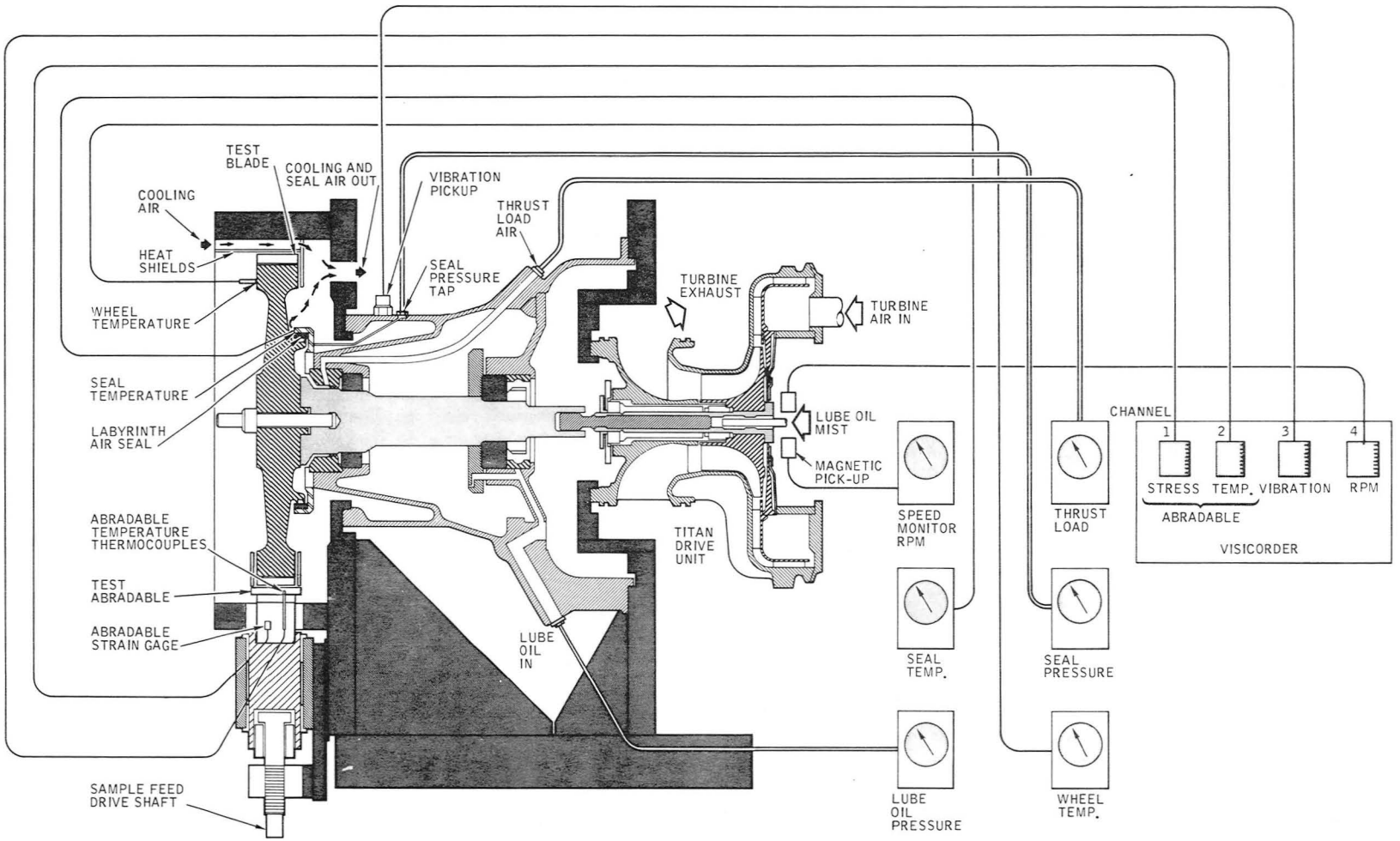

Figure 75. Schematic of Seal Test Rig

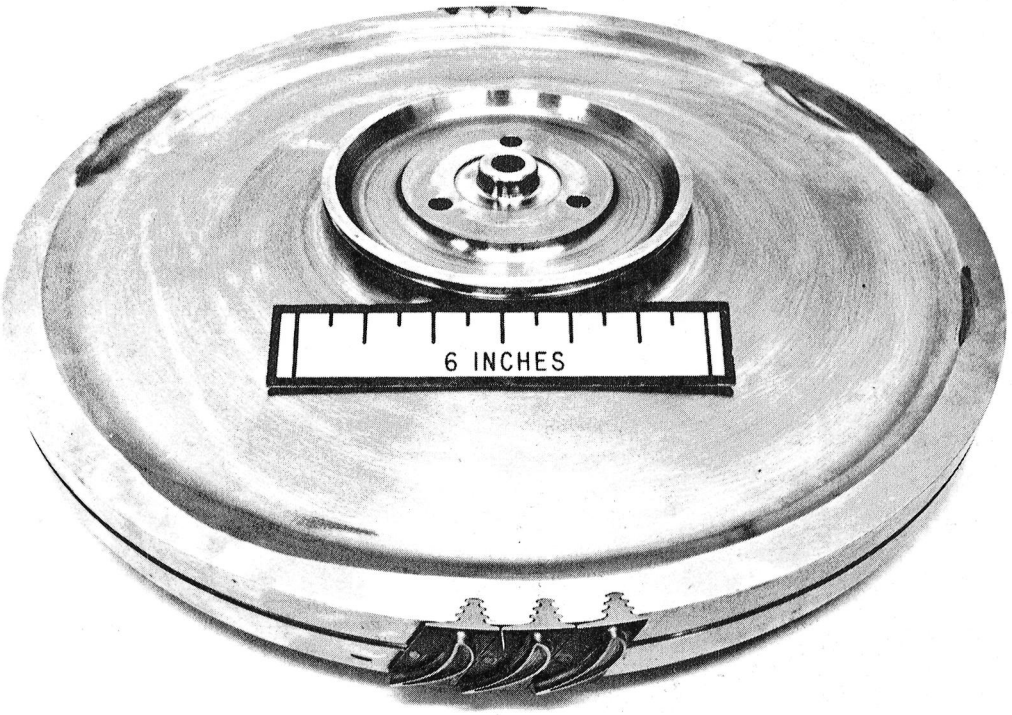

Figure 76. Seal Test Rig Wheel Showing MAR-M421 Alloy Stub Blades

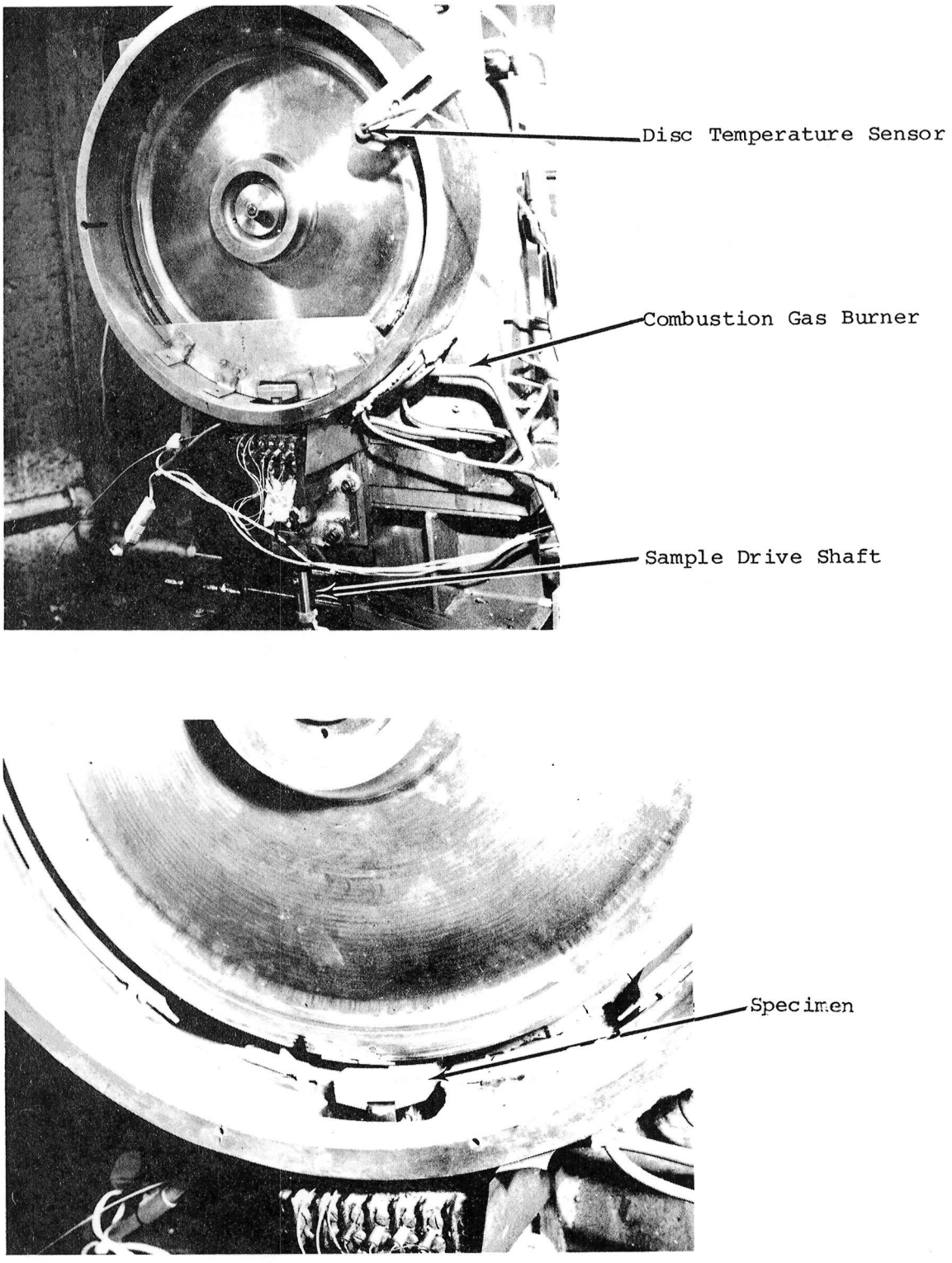

Figure 77. Seal Test Rig Showing Setup for Testing Honeycomb Blade Tip Seals at Elevated Temperature

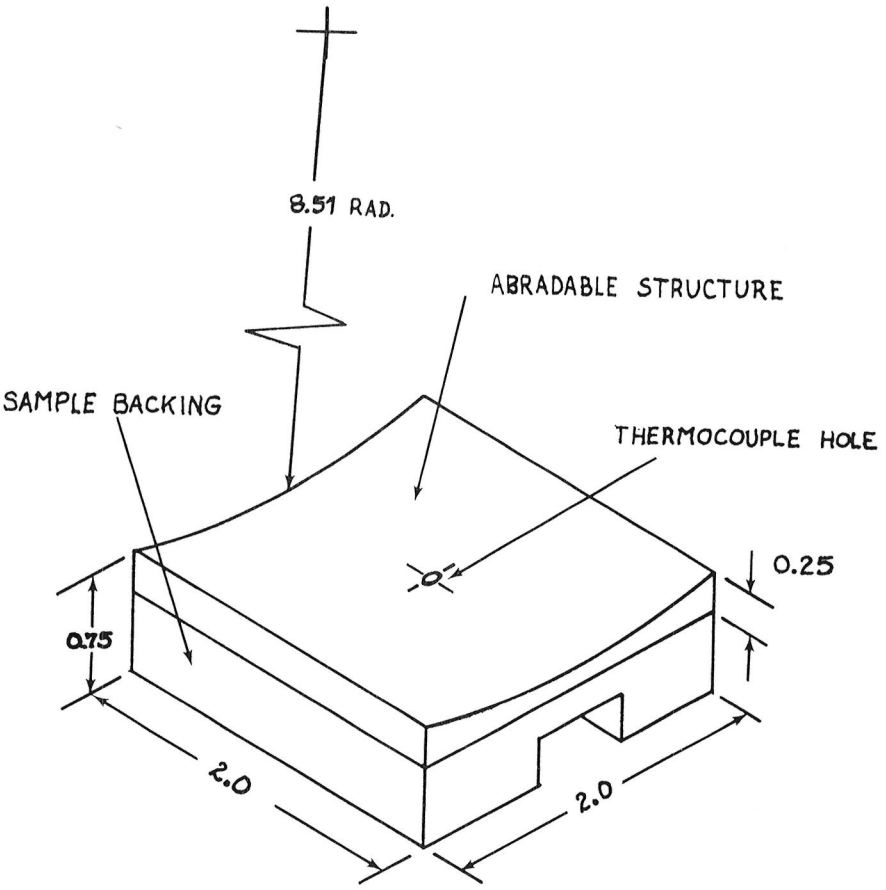

Figure 78. Typical Abradable Seal Sample (Attachment Hubs Not Shown)

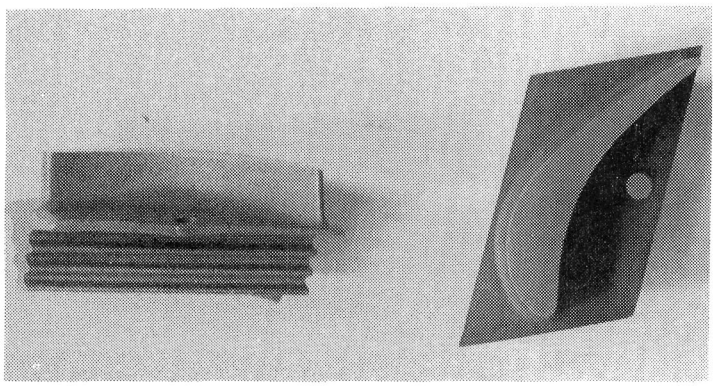

Figure 79.

Standard MAR-M421 Stub Blades Used in Rub Testing

APPENDIX B

BALLISTIC IMPACT TESTING EQUIPMENT

APPENDIX B

BALLISTIC IMPACT TESTING EQUIPMENT

The ballistic impact apparatus, shown in Figure 80, consists of a Crosman 0.22 caliber air rifle modified to accept precise charging with high-pressure air or nitrogen gas prior to each firing. Spherical steel balls are used as the projectiles. Calibration of the rifle for pellet velocity as a function of gas pressure in the rifle is accomplished by means of a commercial ballistic chronograph. In operation the specimen to be tested is secured to a support mounted at the desired location and angle relative to the projectile path. The rifle is then fired at the preset test conditions. After test the impact crater is examined to establish the extent of impact damage.

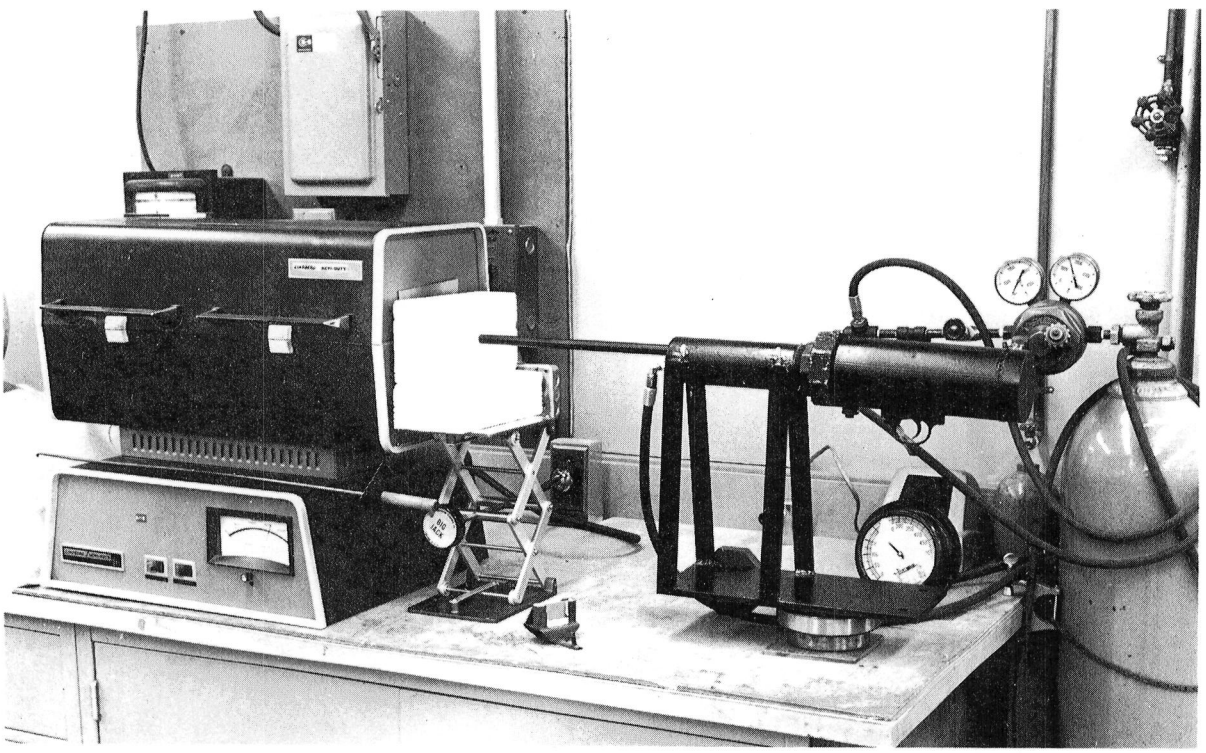

Figure 80. Typical Laboratory Setup for Impacting Ceramic Specimens

The test environment can be adjusted as required by enclosing the specimen in a suitable chamber. The example shown is for elevated-temperature testing.

APPENDIX C

OXIDATION/EROSION RIG

APPENDIX C

OXIDATION/EROSION RIG

Solar has developed several generations of turbine environment simulators for the evaluation of materials without the expense of using a test engine. The rig used in this program includes a high-temperature combustion chamber (fabricated from Hastelloy X) burning kerosene, a nozzle and a sample holder. The sample (50 mm x 50 mm x 5 mm) is held in the gas stream on a water-cooled platform. Surface temperature of the sample is maintained at 1370°C as measured optically during test. Visual observations are made periodically for sample integrity and proper operation. Test duration was 100 hours with sample removed for examination at 24-hour intervals.

A brief description of Solar's burner rigs will be found in the following section.

C.1 COMBUSTION CHAMBER

The design of the burner rig combustors is based on Solar's modern gas turbine combustors. Figure 81 illustrates the straight-through, can-type combustor employing single nozzle fuel atomization, typical in Solar's burner rigs.

The combustion section consists of a preheat section and a main combustion chamber. The preheater operates on natural gas and provides 316 to 427°C air to the main combustor. Thus, the selected fuel, gas or liquid, is combined with the preheated air to provide the high-velocity, hot gas stream. Liquid or gaseous additions are usually introduced in the combustor while solids are injected into the exit nozzle section.

Typical operating conditions for the main combustor are shown in Table 13. Interchangeable combustor cans enable Solar's burner rigs to use either liquid or gaseous fuel. Kerosene, JP-5, Diesel No. 2 and natural gas are currently available. Small 1893-liter tanks are also available for reference fuels, e.g., Diesel No. 2 doped to give one percent sulfur.

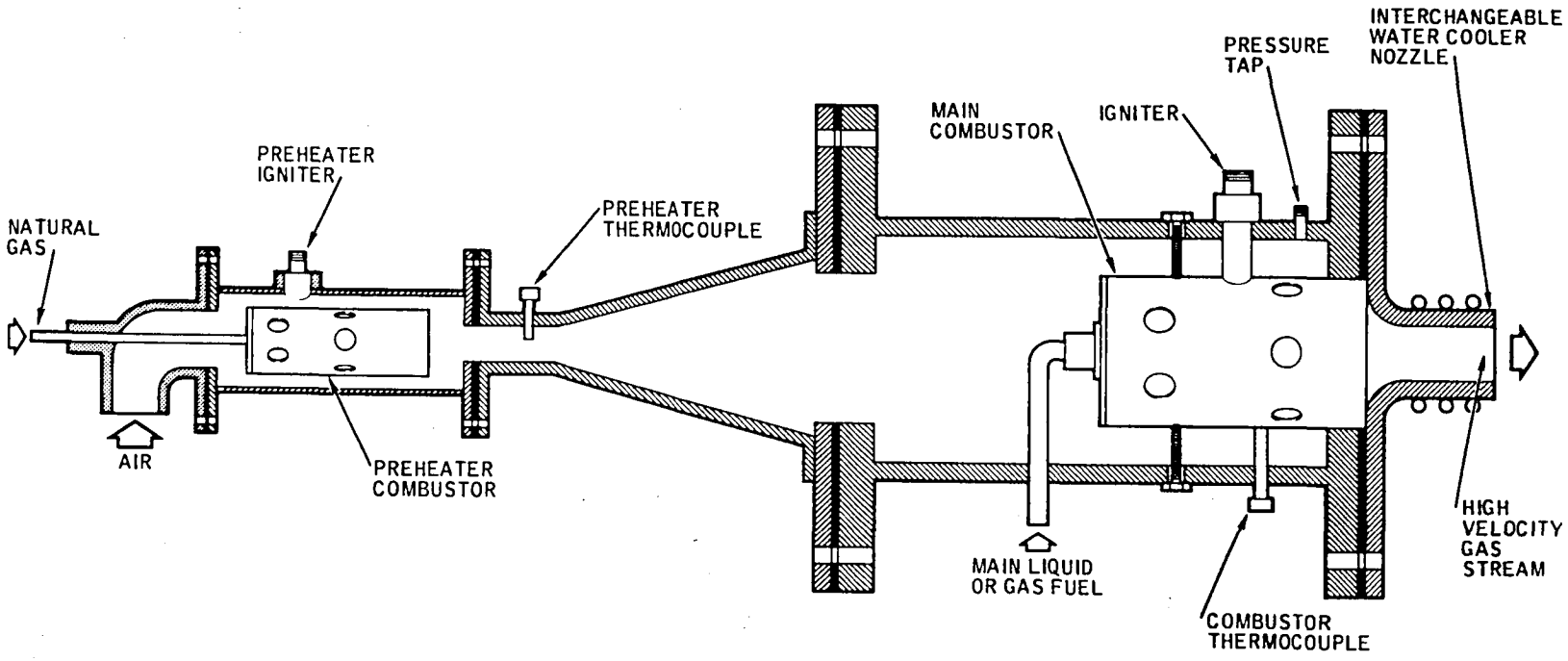

Figure 81. Typical Schematic of Solar Environmental Burner Rig (Vertical and Horizontal Configuration

Table 13

Typical Burner Rig Operating Conditions*

Main combustor inlet air temperature	100 to 425°C
Combustor pressure	205 to 2050 MPa
Air-fuel ratio (liquid fuel)	
Air flow	214 kg/hr
Fuel flow	8 kg/hr
Exhaust gas velocity	183 to 580 m/sec
Exhaust gas temperature	815 to 1425°C
Fuels	Natural gas, Diesel No. 2, kerosene, JP-5 and reference fuels with controlled sulfur

* Values depend on the nozzle attached to combustor exit and the test chamber geometry.

C.2 NOZZLE CONFIGURATION AND TEST CHAMBER

Gases from the combustors exhaust acceleration tubes and impinge on the test samples. The acceleration tubes are used to bring particulates to velocities approaching that of the gas stream.

Test samples are cycled in and out of the gas stream on predetemined cycles to generate periodic heating and cooling stresses such as are encountered in a gas turbine. Automatic timers set the cycling time. Periodically the cycle is interrupted for specimen examination.

REFERENCES

1. Carruthers, W.C., Walker, B.HJ. and Van Wanderham, M.C., "Experimental Analysis of a Hybrid Ceramic - Wrought Superalloy Turbine", ASME Gas Turbine Conference (March 1977).

2. Uy, J.C., Williams, R.M., and Swank, L.R., "Design Properties of Silicon Nitride for High-Temperature Gas Turbine Applications", ASME Gas Turbine Conference (March 1977).

3. Weibull, W., "Statistical Theory of Strength of Materials", Proceedings of Royal Academy of Engineering Science, No. 151 (1939).